Equilibrium and stability studies of oblate field-reversed configurations in the Magnetic Reconnection Experiment

S. P. Gerhardt, E. Belova, M. Inomoto,[a] M. Yamada, H. Ji, Y. Ren, and A. Kuritsyn
Princeton Plasma Physics Laboratory, Princeton, New Jersey 08543

The equilibrium and stability of oblate field-reversed configurations (FRCs) have been studied in the Magnetic Reconnection Experiment [M. Yamada *et al.*, Phys. Plasmas **4**, 1936 (1997)]. In the absence of a passive stabilization, tilt and shift instabilities often become unstable, with the tilt in particular limiting the plasma lifetime. The tilt instability can be mitigated by either including a passive stabilizing conductor, or by forming very oblate plasmas. Large perturbations ($n=2$ and 3) may still remain after passive stabilization is applied. These perturbations have the characteristics of co-interchange modes, which have never been observed, and can lead to the early termination of the plasma. The co-interchange modes can be minimized through the formation of plasmas with a very oblate shape, leading to the maximum FRC lifetime. A code has been developed to calculate equilibria for these plasmas. A rigid-body model explains the improved stability of oblate plasmas to $n=1$ tilt modes. Numerical calculations indicate improved stability to $n \geq 2$ co-interchange modes for the very oblate plasma shapes. © *2006 American Institute of Physics*.
[DOI: 10.1063/1.2360912]

I. INTRODUCTION

The field-reversed configuration[1] (FRC) is a toroidal plasma configuration with toroidal plasma current, but negligible toroidal field. This configuration has many advantageous features for the core of a fusion power plant, including intrinsically high β, a simply connected geometry, and a natural divertor structure.[2] The FRC has the further advantage that it can be robustly translated along a guide field,[3–5] separating the formation region from the fusion burn region.[2,5] These advantages, however, have been balanced against great theoretical concerns about the magnetohydrodynamic (MHD) stability of these configurations.[6–29] The traditional prolate (axially elongated) FRC is predicted to be MHD unstable to the $n=1$ internal tilt instability,[6–20] where the plasma displacement is localized internal to the plasma boundary (n is the toroidal mode number). This instability occurs when the plasma current ring tilts to align its magnetic moment to the external magnetic field, and is predicted to grow on the Alfvén transit time. Although the mode has not been conclusively identified in experiment,[30,32,33] it presents a potential obstacle in the path toward a FRC reactor.

Concern about these instabilities has motivated recent theoretical[13,14,16] and experimental[34–37] studies of FRCs with a more spherical plasma boundary. These oblate FRCs have an elongation $E < 1$ ($E = Z_S/R_S$, with Z_S and R_S the separatrix half-length in the axial direction and separatrix radius, respectively; prolate FRCs typically have $E \approx 3-10$). Oblate configurations are predicted to have different and potentially advantageous stability properties compared to prolate FRCs. The tilt mode in these configurations becomes an external mode, where the plasma boundary moves significantly; the change in mode character from internal to external allows it to be stabilized by nearby passive conducting structures. Further, these oblate configurations maximize the shortest distance between the hot plasma core and the cool plasma edge. The larger major radius of these configurations may further improve the confinement, if the R^2/ρ_{i0} scaling of the particle confinement time from prolate FRCs[38] holds for the oblate case (R is the major radius and ρ_{i0} is the ion-gyroradius in the external field).

However, even in the presence of passive stabilization, these oblate FRCs (and prolate FRCs as well) are predicted to be unstable to co-interchange modes,[23–29] which are $n \geq 2$ cousins of the tilt mode.[1,16,28] These co-interchange modes have never been identified and studied in an experiment, and represent a fundamental uncertainty with regard to the reactor prospects of oblate FRC plasmas.

We have conducted a series of oblate FRC experiments in the Magnetic Reconnection Experiment (MRX)[39] in order to explore these issues. We have found that without a passive stabilizer, the plasma develops $n=1$ tilt or shift modes, depending on the external field configuration. The dangerous tilt mode was mitigated by two methods: (1) by the installation of a passive stabilizer, in the form of a hollow conducting center column, and (2) by forming very oblate plasmas. The radial shift mode was stabilized by the center column. Without the center column, the growth of the shift-mode was limited, apparently by the large magnetic fields on the outboard side of the device.

Although the stabilizer helped in eliminating $n=1$ modes, dangerous co-interchange modes with $n \geq 2$ remained. This represents the first experimental observation of these instabilities. Forming an extremely oblate plasma leads to minimal amplitude of these $n \geq 2$ modes and the maximum plasma lifetime. Thus, this series of experiments has demonstrated the importance of *both* plasma shape and passive stabilization for optimum oblate FRC performance.

[a]Present address: Osaka University, Osaka, Japan.

13, 112508-1

We have developed a MHD equilibrium code to study these plasmas. The code solves the Grad-Shafranov equation, subject to the available constraints. The vacuum vessel is treated as a perfect flux-conserver in this modeling, allowing a fast and convenient Green's-table approach to computing the equilibria and predicting the diagnostic signals. The calculations have demonstrated the means through which the plasma shape can be modified and controlled by external field shaping.

These equilibria have been used to predict the stability properties of FRCs in MRX. A rigid body stability model is used to predict the tilt/shift stability of the FRC. This model predicts that the plasma should be in the tilt unstable regime when the plasma shape is sufficiently oblate, in approximate agreement with the measurements. Simulations with the hybrid and MHD (HYM) stability code[15] indicate a reduction of the MHD linear growth rate of both radially and axially polarized co-interchange modes at large mirror ratio, a result that is confirmed by a simple analytic model.[29] Nonlinear simulations confirm that the radially polarized instabilities are largely suppressed by the unique external field configuration of MRX.

The remainder of this paper is organized as follows. A brief review of relevant stability expectations, based on both theory and experiment, is given in Sec. II. A detailed description of the experimental apparatus is given in Sec. III. Our experimental measurements are presented in Sec. IV. The results of our equilibrium fitting calculations are given in Sec. V. Stability calculations for the FRC plasmas in MRX are presented in Sec. VI including both a rigid body model for the tilt/shift instability and three-dimensional (3D) MHD simulations using the HYM code. A discussion of our conclusions is presented in Sec. VII. Appendix A presents some details about the equilibrium fitting algorithm, and Appendix B illustrates a stability analysis based on local-mode theory.

II. STABILITY EXPECTATIONS FOR OBLATE FRCs

This section provides a brief introduction to relevant topics in FRC stability. The stability of both the well-studied prolate FRC and the less-studied oblate FRC is reviewed, from theoretical and experimental perspectives. The goal of the review is to introduce the new reader to the issues in oblate FRC stability, and to relate the properties of oblate FRCs to their more commonly known prolate cousins. No claim is made that the review is comprehensive; a thorough review of prolate FRC stability can be found in Ref. 1.

The theoretical stability studies of these plasmas can generally be divided into two classes: (1) studies of the $n=1$ tilting/shifting instabilities[6–20] and (2) studies of local stability in the $n\gg1$ limit.[21–29] A few studies have bridged the gap between these two limits.[12,16,17] Note that studies of ion-ring[40] plasmas, which are in many ways similar to oblate FRCs, have examined the stability of co-interchange modes,[41–43] as well as $n=1$ tilt stability.[44]

The $n=1$ internal tilt mode is the most heavily studied instability in the prolate FRC literature. The growth rate for this instability is predicted to scale as $\gamma=CV_A/Z_S$, where V_A is the Alfvén speed defined in terms of the separatrix field and the maximum density, and C is a constant of order unity. No nonlinear saturation of the internal tilt was found in MHD or Hall-MHD simulations,[12] and only very high toroidal rotation speeds were found to be stabilizing.[9,11] This internal tilt mode is predicted to become stable when the separatrix elongation is reduced below one, but an external tilt then becomes unstable.[6,13,14,16] This external tilt may be preferred compared to the internal version, as it can be more easily stabilized by nearby conductors.[16] Further, the external tilt should be stabilized for very low elongation ($E\sim<0.5$), even without a passive stabilizer.[14,16] The $n=1$ radial shifting instability is expected to become destabilized for $E<\sim1$,[14,16] but can also be stabilized by nearby conducting structures.

Given the intense theoretical interest in the internal tilt in prolate FRCs, it is interesting to note that there is little experimental evidence of its existence. Measurements in Field-Reversed Experiment-C/Large Source Modification (FRX-C/LSM) indicated a degradation in confinement, which was correlated with tilt-like magnetic perturbations measured at the chamber wall.[30,31] However, subsequent studies in the Large-s Experiment[32,33] were unable to establish the presence of the tilt instability. Further, FRCs formed in theta-pinches[1] have been shown to exist for much longer than an Alfvén transit time.[45] The conventional explanation for this apparent stability was the presence of finite Larmor radius (FLR) effects.[10,46] The parameter $\bar{s}$ (the approximate number of ion gyroradii between the plasma edge and the field null) is defined as

$$\bar{s} = \int_{R_0}^{R_S} \frac{r}{R_S \rho_i} dr. \tag{1}$$

Here, R_s is the separatrix radius at the midplane, R_0 is the radius of the field null, and ρ_i is the ion gyroradius. Kinetic effects are considered to be important is stabilizing the tilt mode when $\bar{s}/E < 0.2-0.5$.[16,31] Most theta-pinch formed prolate FRCs to date have operated in this regime.

More recent theoretical research on prolate FRCs has indicated that although FLR effects by themselves are capable of reducing the linear growth rate of the internal tilt, they are not sufficient to entirely eliminate the instability.[17,18] On the other hand, the nonlinear saturation of the $n=1$ tilt at finite amplitude has been observed in kinetic regime simulations.[19] Hence, it is as yet unclear if the internal tilt mode would be a problem in a prolate MHD-regime FRC reactor. This uncertainty regarding the internal tilt has been a major motivation for the present oblate FRC studies, where the external tilt can be stabilized by external conducting structures.

The second class of extensively studied instabilities are the $n\gg1$ local modes. The stability criterion for $n\gg1$ interchange instabilities was found in early research:[21]

$$(V''/V' + p'/\Gamma p) > 0. \tag{2}$$

In this equation, V is the plasma volume, p is the pressure, Γ is the ratio of specific heats, and the primes represent derivatives with respect to poloidal flux (ψ). In the FRC context, an
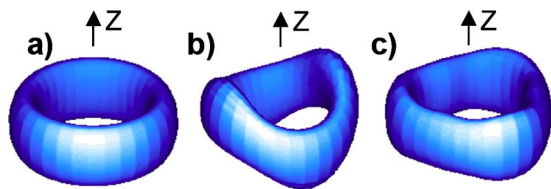
FIG. 1. (Color online) Examples of numerically computed co-interchange displacements. The z axis (axial direction) is indicated with an arrow. The unperturbed pressure isosurface is shown in (a). The results of $n=2$ axial mode are illustrated in (b), and an $n=3$ radial mode in (c).

interchange instability has a displacement normal to the constant ψ-surface ($X \propto rB\vec{\xi} \cdot \vec{\nabla}\psi$, with ξ a small displacement[21]) that is constant along a field line. Profiles that are nominally stable to these interchange modes have been found, for both oblate[16] and prolate[22] FRCs. Further research identified a class of co-interchange modes,[23–29] which are the $n>1$ equivalent of the tilting/shifting modes.[28] These incompressible modes have the dominant displacements localized in the region of largest curvature (ballooning-like), and have a growth rate comparable to the inverse Alfvén transit time.[23] The incompressible co-interchange modes are often faster growing than the interchange mode, which have the stabilizing effect of compressibility.[23,28]

The stability of intermediate-n ($1<n<8$) co-interchange modes in an oblate FRC was studied in detail by Belova *et al.*[16] In that study, the co-interchange modes were broken into two classes, using a naming convention from Ref. 43 that will also be used in this paper. Axially polarized co-interchange modes have fluid displacement prominently in the z direction. The $n=1$ version of this mode is the tilt mode. An example of this type of mode is illustrated in Fig. 1(b) for $n=2$, where the pressure isosurfaces calculated by the HYM code are plotted. Radially polarized co-interchange modes have the displacement prominently in the radial direction.[16] The $n=1$ version of this mode is the radial shift mode. An example of this type of instability is plotted in Fig. 1(c), for the $n=3$ radially polarized co-interchange mode. The calculations have indicated that both polarizations of modes could be simultaneously unstable in an oblate FRC. These co-interchange modes were computed to become more localized to the field null as the mode number increases, causing them to be less sensitive to the presence of nearby conducting structures. Further, FLR stabilization of these intermediate-n modes was predicted to be inefficient due to their large growth rate,[16] unlike the prolate case.[17,18] These modes typically grew until the configuration was destroyed. Recent computational studies have demonstrated that the presence of a nonthermal ion population can stabilize the co-interchange modes in an oblate FRC.[20] Despite this considerable theoretical interest in the co-interchange mode, they have never previously been experimentally observed.

It is interesting to compare these FRC instabilities to those of other plasma configurations. The tilt/shift modes are the direct analogy of the $n=1$ kink modes in the pure Z pinch,[47,48] where the FRC is "unwound" into a linear configuration and the poloidal field of the FRC becomes the azimuthal field of the pinch.[1,33] The co-interchange modes are the analogy of higher-n kink modes. Similarly, the FRC interchange is analogous to the Z-pinch sausage mode.[33] Furthermore, the $n=1$ tilt/shift modes in an FRC have many similarities to the $n=1$ tilt/shift modes in a spheromak.[7,14] Although two configurations have very different equilibrium states, the stability to the $n=1$ modes is largely determined by the interaction of the toroidal plasma current with the coil currents producing the external field. Finally, the oblate FRC tilt/shift and co-interchange modes are very similar to instabilities in ion-ring plasmas.[26,41–44]

The kink-like co-interchange is *not* analogous to the tokamak external kink, which is driven by gradients in the toroidal current profile and requires a rational surface between the plasma boundary and the conducting wall.[49] The helical pitch of the tokamak external kink eigenfunction is determined by the rational surface in the vacuum region outside the plasma; the axially and radially polarized co-interchange modes in an FRC may be superposed to form a helical structure, but the modes themselves are independent eigenfunctions of the ideal MHD equations. In terms of tokamak instability, the co-interchange most closely resembles the tokamak ballooning mode, but without the stabilizing influences of magnetic shear and good curvature.[50]

It should be noted that in the present prolate FRC experiments, the $n=2$ rotational mode[31,33,51–54] is the instability that typically leads to the termination of the discharge, unless some additional stabilization method is employed.[52–54] This mode causes a rotating elliptical distortion of the plasma boundary (is radially polarized), and can destroy the FRC when the distorted plasma boundary comes in contact with the confinement chamber.[51] Successful stabilization methods include the use of a quadrapole stabilizing field,[52,53] and the effects of a rotating magnetic field (RMF).[54]

The experimental study of oblate FRCs began with the "nearly spherical" FRCs described in Nakata *et al.*[55,56] These experiments use the combination of a double-cusp bias field, a laser produced plasma, and fast rising coils to form the FRC. The plasma exhibited gross stability to rotational and tilt modes, which were attributed to field line bending and FLR effects, respectively.[56]

The TS-3 device pioneered the process of forming FRCs via the counter-helicity merging of spheromaks,[57] and these experiments have continued in the up-scale TS-4 device. These experiments have demonstrated the importance of two-fluid effects in the relaxation of the plasma to an FRC state,[34,36] and the role of shear flow in stabilizing $n=1$ tilt instabilities.[35] These experiments utilized a conducting central column to stabilize the tilt/shift instability,[36] without a detailed study of its effect on the configuration.

The Swarthmore Spheromak Experiment (SSX) has also studied nearly oblate FRCs formed by spheromak merging,[37] focusing on a novel configuration with large antisymmetric toroidal fields.[58,59] These unique FRCs were confined within a flux conserver; the aspect ratio of this flux was chosen such that the FRC would be unstable to tilting. The external tilt was indeed observed, although the time-scale for the tilt to develop was significantly longer than the MHD prediction. This improved stability is thought to be due to the large viscosity and line-tying in these experiments.[60]
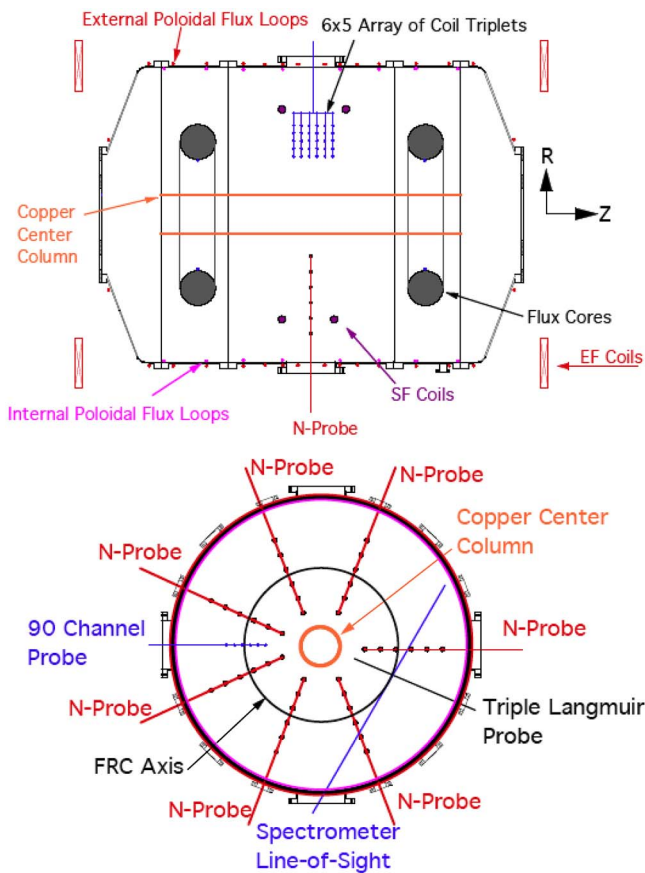
FIG. 2. (Color online) Side view (a) and end-on view (b) of the MRX device.

steady state "EF" coils provide additional external field, and the shaping-field coils (the "SF" windings) are utilized to control to details of the plasma shape. These different coils allow us to vary the mirror ratio (MR) of the external field, defined as

$$\mathrm{MR} = \frac{B_Z(R = 0m,\ Z = 0.55m)}{B_Z(R = 0m,\ Z = 0m)}. \tag{3}$$

FRCs formed in a field with a large mirror ratio tend to be more oblate (lower elongation). Plasmas formed in a lower mirror ratio field tend to be more prolate (larger elongation), though the elongation is never greater than ~0.6 in the MRX plasmas generated to date. Note that the actual external field distribution may be significantly different from that of a simple mirror field; the mirror ratio is a simple means to describe the otherwise complicated external field.

MRX utilizes two distinct sets of magnetic probe[72] arrays for FRC studies, both of which are illustrated in Fig. 2. The "90-channel" probe array is a 6×5 array of coil triplets at fixed toroidal angle, with 4 cm resolution. By scanning this probe in the radial direction between discharges, it is possible to develop a two-dimensional picture of the FRC evolution at this toroidal angle. A second 105-channel probe array is composed of seven linear probe arrays, each with five coil triplets spaced by the 8 cm. These seven probes are inserted at different toroidal angles (approximately equally distributed in toroidal angle), but to the same radius. This array allows us to measure the midplane magnetic perturbations with toroidal mode number up to $n=3$, for all three components of the magnetic field; these probes are thus referred to as "N-probes."

In addition to the magnetic probe arrays, an array of 16 flux loops external to the vacuum vessel has been constructed. These loops provide an important measurement of the amount of poloidal flux leaking out from the vacuum vessel. The data from these loops will be important in justifying the flux-conserving vessel model in Appendix A.

The kinetic information collected in MRX has been more limited. A triple Langmuir probe[72] is used to measure the electron temperature and density as a function of time, but at a single point. This point was typically near the magnetic null of the FRC plasma. Doppler spectroscopy[73] was utilized to measure the temperature of He^{+1} or Ne^{+1} along a chord through the center of the plasma. The light was measured utilizing a CCD camera, with a single $10-20\ \mu s$ exposure collected per discharge.

We have successfully formed FRC plasmas in deuterium, helium, neon, and argon in MRX. This paper will focus mainly on helium plasmas, where the ion temperature can be easily measured with spectroscopic techniques. The parameters for the FRCs formed in the mirror ratio scans are illustrated in Table I. The quantities that require knowledge of the FRC equilibrium properties (such as the elongation) are derived from the equilibrium fitting, as described in Sec. V and Appendix A. These plasmas *do not* satisfy the relationship $\bar{s}/E < 0.2-0.5$, and are thus in the MHD regime with regard to the tilt instability.[18,31]

Note that the external tilt-instability was indeed observed in the TS-3/4 and SSX oblate FRC experiments, in contrast to the prolate case in which the internal tilt has not been conclusively observed. Tilting instabilities have also been clearly identified in oblate spheromak plasmas, which as noted above, are closely analogous to the tilt-modes in oblate FRCs.[61–63] These spheromak tilt instabilities have been controlled through the use of figure-8 coils,[63,64] or by forming the spheromak in a flux conserver with appropriate aspect ratio.[62]

III. THE MRX APPARATUS

MRX is a flexible facility for the study of both compact toroids and the basic physics of magnetic reconnection.[65–70] The facility was designed with both types of experiments in mind, with the physics of magnetic reconnection receiving the majority of experimental attention. The infrastructure created for these reconnection science experiments has created a firm foundation upon which to build for the present FRC studies.

The primary flexibility in the MRX device[39] for FRC studies is derived from the three coils sets that contribute to the external field, as illustrated in Fig. 2(a). The spheromaks are formed using an inductive flux-core formation scheme.[71] After spheromak formation, the toroidal windings of the flux-cores (the poloidal field, or "PF" windings) are utilized to produce a portion of the confining external field. The large

TABLE I. Parameters for the helium FRCs discussed in this paper.

Fill pressure (mTorr)	7–9.7
Density (cm^{-3})	$(0.5-2) \times 10^{14}$
Ion temperature (eV)	~ 18
$B_{Z,\mathrm{Sep}}$ (G)	300–200
Elongation, E	0.65–0.35
$\bar{s}$	3–1
$\bar{s}/E$	5–2

IV. MEASUREMENTS OF OBLATE FRC STABILITY IN MRX

We have conducted systematic studies of the stability properties of oblate FRCs in MRX. This section begins with a classification of the instabilities in Sec. IV A, followed by a description of the evolution of example discharges in Sec. IV B. The detailed dependence of the magnetic perturbations on the plasma shape and passive stabilizer is presented in Sec. IV C, and the impact of the instabilities on the plasma lifetime is described in Sec. IV D.

A. Magnetic perturbation structures in FRCs in MRX

The toroidally distributed probe array provides information about midplane magnetic perturbations with good resolution in both time and space. This information has been used in conjunction with HYM code simulations to identify the observed perturbations. These have been identified as $n=1$ tilting/shifting, or the higher-order $n \geq 2$ co-interchange modes.

The simulated magnetic perturbations at $Z=0$ are plotted in Fig. 3(a) for the $n=3$ radially polarized co-interchange, and Figs. 3(b) and 3(c) for the $n=2$ axially polarized co-interchange (the linear mode structure is shown). These magnetic perturbations are from the same calculations as were used to compute the distorted pressure isosurfaces in Fig. 1. For the $n=3$ radially polarized case in Fig. 3(a), the plasma moves radially inward or outward. This causes an alternatively positive then negative perturbed B_Z field. There is a negligible perturbation to B_R or B_T at the midplane in this case. The axially polarized co-interchange produces perturbations to B_R and B_T, as illustrated in Figs. 3(b) and 3(c). These perturbations are caused by the axial motion of the
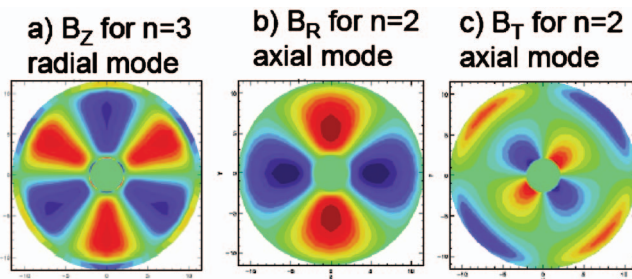

FIG. 3. (Color) The computed midplane magnetic perturbations for $n>1$ co-interchange modes. The B_Z perturbation for the $n=3$ radial mode is illustrated in (a), and the B_R and B_T perturbations for the $n=2$ axial mode is shown in (b) and (c).
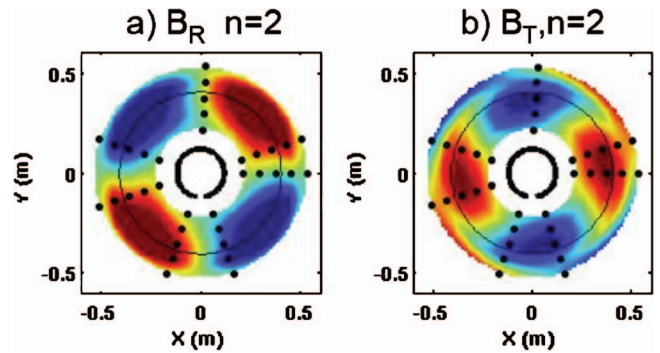

FIG. 4. (Color) The measured (a) B_R and (b) B_T perturbations in MRX, for $n=2$.

plasma dragging the FRC poloidal field into the midplane. There is a negligible B_Z perturbation in the midplane due to this mode.

The computed perturbations have properties similar to the measured perturbation structure in MRX. The measured midplane magnetic perturbation is expressed as a Fourier series of the form

$$B(R,\phi) = B_0(R) + \sum_{n=1}^{3} \left[C_n(R)\cos(n\phi) + S_n(R)\sin(n\phi) \right].$$

(4)

This expression is fit the N-probe array data at each of the five radial locations of the probe triplets, yielding the fit coefficients $B_0(R)$, $C_n(R)$, and $S_n(R)$ at five radial locations. We then radially interpolate these fit coefficients in order to determine the radial dependence of each distinct Fourier mode. These interpolated Fourier coefficients are then used to calculate the magnetic perturbations at all locations in the midplane.

The distribution of the $n=2$ midplane B_R and B_T perturbations are illustrated in Fig. 4. These have striking similarity to those in Figs. 3(b) and 3(c). There are strong and *global* B_R perturbations in this example, as in the computation in Fig. 3(b). The maximum of the B_T perturbation lies between the B_R maxima. Similar observations have been made for the B_Z perturbations, which show great similarities to the simulation in Fig. 3(a).

These observations lead to an interpretation of the N-probe data in terms of the axially and radially polarized co-interchange modes. The B_R perturbation represents the axially polarized modes, with the B_R, $n=1$ perturbation indicative of the tilt mode.[74] The B_Z perturbations are representative of the radially polarized modes, with the $n=1$, B_Z perturbation indicative of the radial shift mode.

Note that there are caveats about the above measurement/computation comparison. The simulated magnetic perturbations are for the linear phase of the instability, while the measurements may be of the nonlinear phase. If there is residual B_T in the FRC, the axial and radial modes become coupled, leading to a mixture of all field components at the midplane. Further, the Hall effect, which breaks symmetries present in MHD, tends to distort the mode patterns compared to the MHD structure.[12,18] Nevertheless, the

present interpretation provides simple intuitive rules for the interpretation of the magnetics signals, and will be utilized throughout this paper.

The FRC plasmas in MRX do not display the signs of fast rotation, as measured by both the magnetic perturbation rotation and Doppler spectroscopy. We thus infer that any radially polarized modes we observe are not rotational modes, but instead the radially polarized co-interchange.

B. Example comparisons of more and less stable discharges

We have observed that the plasma stability and lifetime is highly dependent on the presence of the stabilizer and the plasma shape. Many of these trends, which constitute the core of our experimental results, are illustrated in Fig. 5. This figure illustrates the evolution of three discharges: an unstable discharge without a center column (black lines and letters), an unstable discharge with the center column (red lines and letters), and an optimized discharge with the center conductor (blue lines and letters). The "pictures" in Figs. 5(a)–5(l) of the plasma evolution were generated by scanning the 90-channel probe through three radial location during repeatable merging (>7 discharges are used to make these figures). The three frames at the bottom illustrate the evolution of the poloidal flux, B_R $n=1$, and B_R $n=2$ modes. Note that the data in Fig. 5(m) show the individual traces from the many discharges, indicative of the reproducibility, while that in Figs. 5(n) and 5(o) show only the average evolution. The gray areas correspond to the time before the merging is finished.

The discharge in Figs. 5(a)–5(d) is a case with small mirror ratio (MR=2.4), and without the stabilizing center column. This discharge develops a large B_R, $n=1$ mode, as illustrated in the black curve of Fig. 5(n). We interpret this as a tilt mode, which begins to grow even before the merging process is finished. This instability leads to the immediate termination of the configuration. Note the poor reproducibility of these plasmas in Fig. 5(m), due to their inherently unstable nature. The discharge in Figs. 5(e)–5(h) has a similar mirror ratio (MR=2.5), but also has the conducting center column present. The $n=1$ mode is stabilized by the center column in this case, but a large B_R, $n=2$ mode grows immediately after merging is completed [red curve in Fig. 5(o)]. This $n=2$ mode, which we interpret as the axially polarized co-interchange, leads to the termination of the configuration. The discharge in Figs. 5(i)–5(l) is seen to last for considerably longer than the previous two examples. This case has the center column and a larger mirror ratio of 3.4. The $n=1$ and 2 modes do not grow after merging is finished, and the plasma decays without violent instability. This example illustrates that both passive stabilization and plasma shape control play an important role in the formation of improved stability FRCs. The detailed equilibrium properties of these discharges will be presented in Sec. V (see Fig. 12 for the computed equilibria for these discharges).

The final combination of stabilizing mechanisms, i.e., large mirror ratio but no center column, will be discussed further in Sec. IV D. In this case, the tilt is stabilized by the
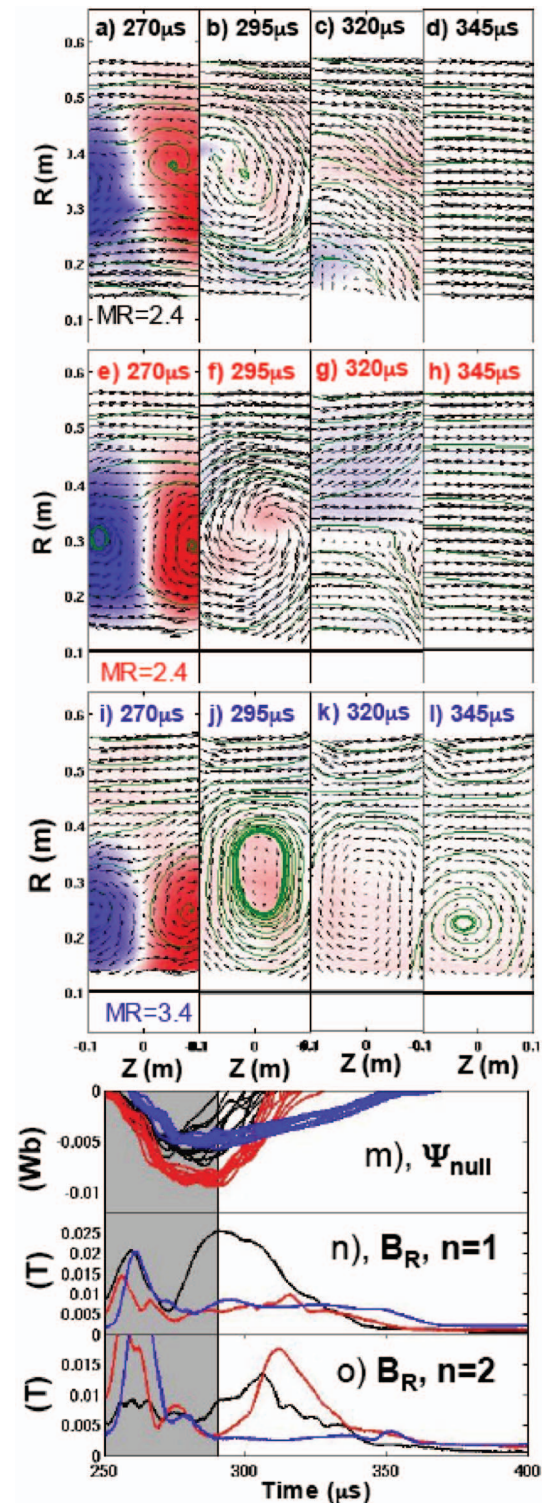

FIG. 5. (Color) The time evolution of three discharge sets is illustrated in (a)–(l). Colors represent toroidal field, arrow represent poloidal field, and a few streamlines are shown in green to guide the eye. The horizontal black line in (e)–(l) indicate the presence of the center column. The bottom section illustrates (m) the poloidal flux evolution, (n) the B_R, $n=1$ evolution, and (o) the B_R, $n=2$ evolution. The colors of the traces correspond to the colors of the letters above. Note the different scales in (n) and (o). See text for further details.

strong shaping, but an $n=1$ shift mode begins to grow. This shift saturates, apparently due to the strong axial magnetic field between the shaping coils, and the plasma often reflects from this high-field region.
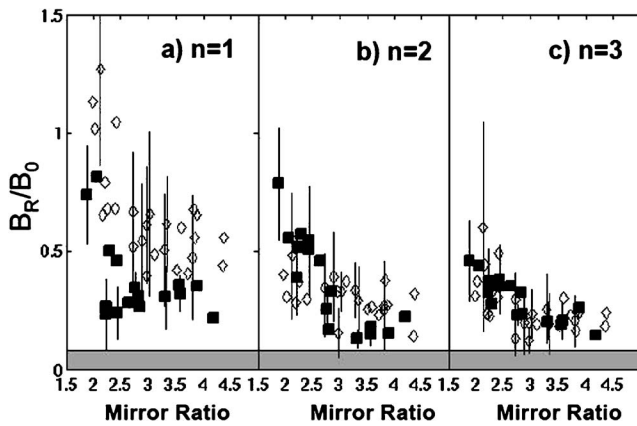
FIG. 6. Magnitude of (a) the $n=1$, (b) the $n=2$, and (c) the $n=3$ perturbations to B_R (axially polarized mode) at $R=0.215$ in the midplane, for helium discharges. The open symbols are for cases without the center column, and closed symbols for cases with the center column. Some representative error bars are shown.

C. The dependence of magnetic perturbations on external field shape

We have made systematic measurements of the magnetic perturbation amplitudes as a function of mirror ratio, for plasmas in different gases. These scans have been done for plasmas both with and without a center column, yielding a detailed picture of the factors that determine the magnetic perturbation amplitudes. These factor are found to be (1) the presence/absence of the passive stabilizer and (2) the degree of oblateness of the plasma (controlled by the external field mirror ratio).

The magnitude of the B_R perturbations are illustrated in Fig. 6, for a series of helium discharges. The $n=1$, 2, and 3 perturbations are illustrated; the value plotted is the largest perturbation after merging is finished, and the error bars represent the shot-to-shot variation of >7 discharges per point. The gray area at the bottom of the page illustrates the minimum resolution in the measurement. The open symbols are for discharges without a center column, and the closed symbols for discharges with the center column present. The perturbations are normalized to the value of B_Z at the outer (large-R) plasma boundary immediately after the FRC formation is finished.

The midplane B_R perturbations, illustrated in Fig. 6(a), show a strong dependence on both the plasma shape and the presence of the passive stabilizer. For the case without the center column (open symbols), the $n=1$ (tilt) perturbations increase as the mirror ratio is decreased. This is the expected result, as the tilt instability is expected to become stronger when the mirror ratio is small (the plasma is more prolate). When the center column is present (closed symbols), the B_R $n=1$ perturbation is suppressed, except at low mirror ratio. This confirms the theoretical expectation that both passive stabilization and plasma shaping can stabilize the external tilt mode.[14,16] In contrast, the $n=2$ and 3 (co-interchange) perturbations are not significantly changed by the presence of the center column, as illustrated in Figs. 6(b) and 6(c). There
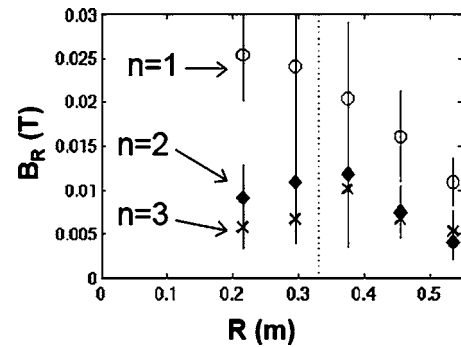

FIG. 7. Radial profiles of the $n=1$, 2, and 3 B_R amplitudes, as a function of minor radius. This case is for a discharge without a center column; the $n=1$ tilt mode has a radially more broad perturbation field than the $n=2$ and 3 axial modes.

is a strong trend toward the reduction of the $n=2$ amplitude as the mirror ratio becomes larger, a trend that is present (more weakly) for $n=3$ as well.

The $n=1$ mode is more strongly impacted by the center column than the other modes due to its broad spatial profile, as illustrated in Fig. 7. This figure shows the radial profiles of the B_R $n=1$, 2, and 3 perturbations as a function of radius, for a set of discharges without the center column. The $n=1$ structure is clearly much broader than the $n=2$ and 3 structures, in keeping with computational predictions.[16] This broader structure allows the mode to interact more strongly with the center column (center column radius is 10 cm), and is thus more susceptible to stabilization.

The B_Z perturbations, indicative of radial displacements, are illustrated in Fig. 8 as a function of the external field mirror ratio. The graphs show discharges with (closed symbols) and without (open symbols) the center column. For the $n=1$ perturbation without the center column, there is a clear trend of increasing B_Z perturbation with increasing mirror ratio. This is in keeping with the expectations that the radial shift should become more unstable as the external field mirror ratio becomes larger (plasma becomes more oblate). The B_Z, $n=1$ perturbations are significantly reduced by the center
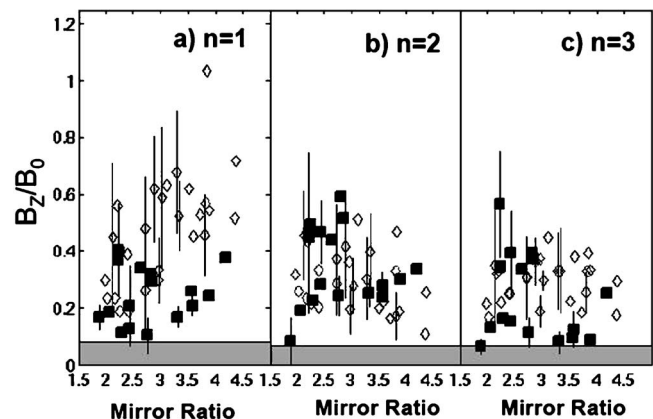

FIG. 8. Magnitude of (a) the $n=1$, (b) the $n=2$, and (c) the $n=3$ perturbations to B_Z (corresponding to radially polarized modes) at $R=0.535$ in the midplane, for helium discharges. The open symbols are for cases without the center column, and closed symbols for cases with the center column. Some representative error bars are shown.
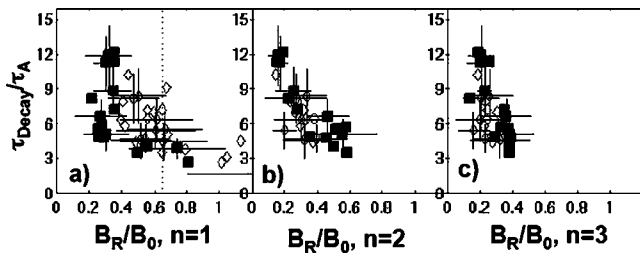
FIG. 9. Plasma decay-time normalized to the Alfvén time, plotted against B_R: (a) the $n=1$, (b) $n=2$, and (c) $n=3$ magnetic perturbations, in helium. The points in (a) with $B_R/B_0 > 0.6$ are not included in (b). Open symbols are for cases without the center column, and closed symbols for cases with the center column.

FIG. 10. Plasma decay time normalized to the Alfvén time, plotted against (a) the $n=1$, (b) $n=2$, and (c) $n=3$ perturbations to B_Z, for helium plasmas. Open symbols are for cases without the center column, and closed symbols for cases with the center column.

column. We observe that the $n=2$ and 3 perturbations are not significantly effected by the presence of the center column or the value of the mirror ratio.

We have also examined the B_T perturbation amplitude as a function of mirror ratio. The trends are very similar to those in Fig. 6. This is as expected for the axial co-interchange mode, which tends to have coupled B_T and B_R perturbations (see discussion in Sec. IV A).

D. The relationship between perturbation amplitude and lifetime

Having established the relationship between the midplane magnetic perturbations and the external field configuration, it remains to demonstrate which of these perturbations is most detrimental to the plasma performance. We do this by studying the plasma decay time as a function of the different perturbation amplitudes. These comparisons will demonstrate that the tilt and axially polarized co-interchange modes must be avoided to form long-lived FRCs in MRX.

There is a strong correlation between B_R perturbations and the e-folding time of the field reversal (used as an indication of the plasma lifetime), as illustrated in Fig. 9. These are helium discha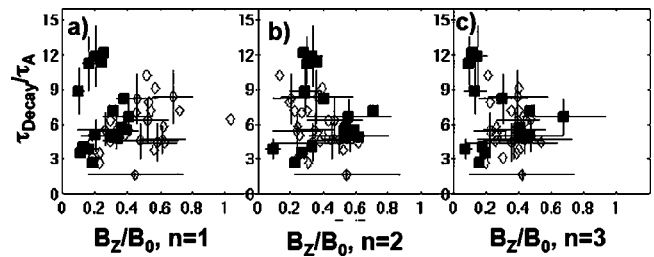rges, and the plasma decay time has been normalized to the Alfvén time ($\tau_A = Z_S/V_A$). As before, the open symbols are for cases without the center column, while the closed symbols are for cases with the center column present. There is a clear trend in Fig. 9(a): when the B_r, $n=1$ (tilt) mode is large, the plasma decay time is short. In this case, the plasma does not decay axisymmetrically, but is instead terminated by the tilt instability. For $B_{R,n=1}/B_0 < 0.5-0.6$, this correlation is reduced. The points with $B_{R,n=1}/B_0 < 0.6$ are replotted in Figs. 9(b) and 9(c), with the x axis corresponding to the normalized $n=2$ and 3 amplitudes. Again, the trend is of decreasing decay time with increasing B_R, $n=2$ amplitude. The decay-time dependence on the $n=3$ perturbation is similar but not as strong. The conclusion is as follows: reducing the B_R, $n=1$ (tilt) amplitude is a necessary but not sufficient condition for a long-lived plasma; large B_R, $n=2$ and 3 co-interchange modes can reduce the plasma decay time even when the $n=1$ tilt is reduced by a combination of plasma shaping and nearby passive conductors. These trends look almost identical if the B_T perturbation is plotted instead of B_R, indicating the coupled nature of these perturbations. This is the expected trend for the axially polarized co-interchange mode.

We observe no correlation between the B_Z perturbation amplitude and the plasma decay-time. The normalized decay
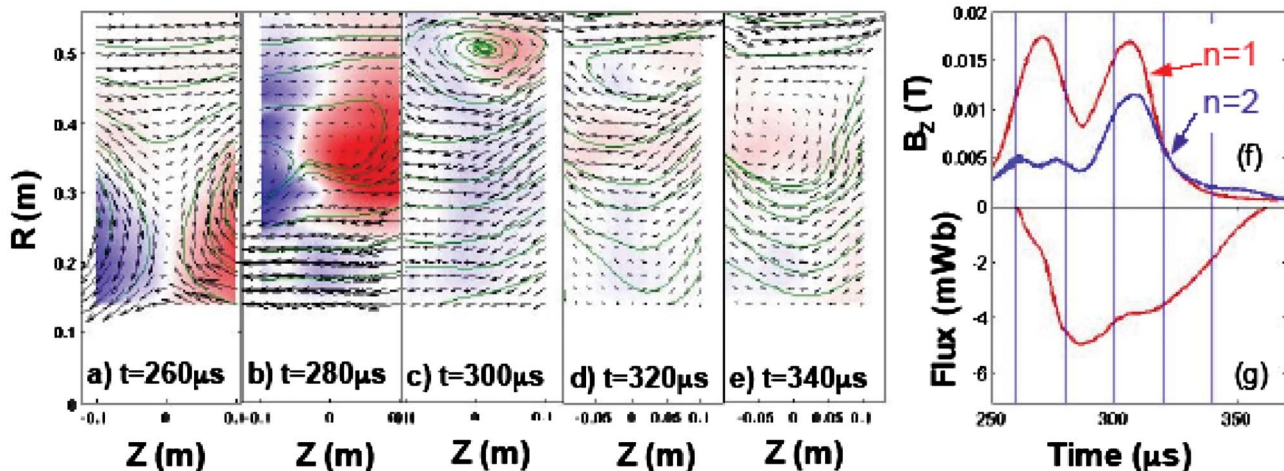

FIG. 11. (Color online) Time evolution of a discharge with a significant $n=1$ radial shift. The frames (a)–(e) illustrate the evolution of the shift at the toroidal angle of the 90-channel probe. A large outward shift of the plasma is visible at $t=300$ μs. The time evolution of the B_Z, $n=1$ and 2 modes is illustrated in (f), and the poloidal flux in (g). Vertical lines indicate the times of the 2D plots. The plasma "bounces" off the high-field region outside the shaping coils; the $n=1$ shift amplitude decreases before the poloidal flux decays away.

time of the helium FRCs is plotted in Fig. 10 as a function of the B_Z, $n=1$, 2, and 3 perturbations. First consider the dependence of the decay time on the $n=1$ perturbations with the center column present (closed symbols). There is no clear dependence of the decay time on the mode amplitude in this case. Long- and short-lived discharges occur for both large and small B_Z perturbations. The data without the center column (open symbols) present the apparent trend of increasing plasma decay-time with increasing B_z, $n=1$ amplitude. The correlation is due to the fact that large B_Z, $n=1$ modes appear at large mirror ratio without the center column, when the tilt is suppressed. These modes do not appear to have a detrimental effect on the plasma; the longest-lived plasmas occur at large mirror ratio where the B_R perturbations are minimized and the B_Z perturbations are often largest. The decay time is apparently uncorrelated with the $n=2$ and 3 radially polarized modes.

It is interesting to consider why the $n=1$ shift is not observed to be destructive in the present MRX plasma parameters and geometry. The two-dimensional evolution of a series of discharges (without the center conductor) with a large shift motion is illustrated in Figs. 11(a)–11(e). These data show that at the toroidal angle of the 90-channel probe array, the plasma shifts radially outward. The toroidally distributed probe array confirms that there is a large $n=1$ perturbation to B_Z, with the plasma shifted out at the toroidal angle of the 90-channel probe. The B_Z, $n=1$ and 2 amplitudes are illustrated as a function of time in Fig. 11(f), and the poloidal flux evolution in Fig. 11(g). We observe that the $n=1$ motion has a peak, after which the plasma appears to "bounce" away from the high-field region outside the SF coils. The $n=1$ amplitude decreases more quickly than the poloidal flux, as the plasma shifts back toward a more centered location. The lifetime of the plasma is not appreciably reduced by this shifting motion. Note that these large shift motions do not occur when the center conductor is present.

V. EQUILIBRIUM RECONSTRUCTION OF OBLATE FRCS IN MRX

In order to facilitate understanding of the stability properties of the FRC, it is necessary to know the detailed structure of the external field, plasma shape and current distribution. Our magnetics measurements are restricted to the midplane for the N-probe array, or to only $Z=\pm 10$ cm and fixed single toroidal angle for the 90-channel probe. Hence, while these diagnostics are extremely useful, neither can provide a complete description of the equilibrium from measurements only.

We have developed the MRXFIT code to overcome this problem.[75] This code uses an iterative technique to solve the Grad-Shafranov (G-S) equation:[49]

$$j_\phi = 2\pi R \frac{dp}{d\psi} + 2\pi \frac{\mu_0}{R} F \frac{dF}{d\psi}, \tag{5}$$

in MRX geometry, subject to all available magnetic constraints. Here, $p(\psi)$ is the pressure profile, which is a function of the poloidal flux, ψ, defined as
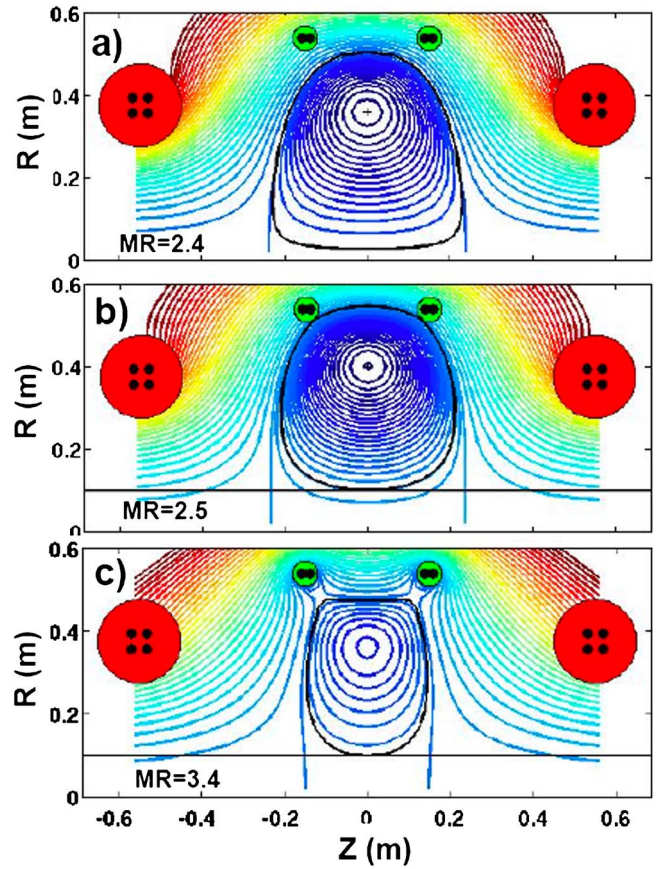

FIG. 12. (Color online) Three example equilibria computed with the MRXFIT code. These equilibria are for the plasmas whose evolution is illustrated in Fig. 5. The case in (a) has an external field mirror ratio of 2.4, but no center column. The case in (b) is limited on the inboard side by the center column. The case in (c) displays the result when the shaping-field coils are used to pull the plasma out, leading to a plasma with a very oblate shape.

$$\psi(R,Z) = 2\pi \int_0^{R'} R' B_Z(R',Z) dR'. \tag{6}$$

The poloidal current stream function $F(\psi)$ is given by

$$F(\psi) = \frac{RB_T}{\mu_o}. \tag{7}$$

The final output of the computation includes the pressure and FF' profiles, which can be used to calculate the toroidal current profile from (5). This is a common MHD equilibrium analysis technique in tokamak,[76–79] reversed field pinch,[75] and spheromak[80,81] research. Note that computational studies of FRC equilibria have been performed,[82–86] but not under the explicit constraint of measurements as described here; the most similar previous equilibrium studies are those in Refs. 84 and 85. The details of the fitting procedure are contained in Appendix A; only the results of the calculation are presented here.

The equilibria for the three different discharges in Fig. 5 are illustrated in Figs. 12(a)–12(c). The case in Fig. 14(a) is for discharge without a center column, and the plasma has a traditional oblate FRC equilibrium. The external field mirror ratio in this case is 2.4, and the plasma elongation is $E=0.48$. As noted previously, this set of discharges developed
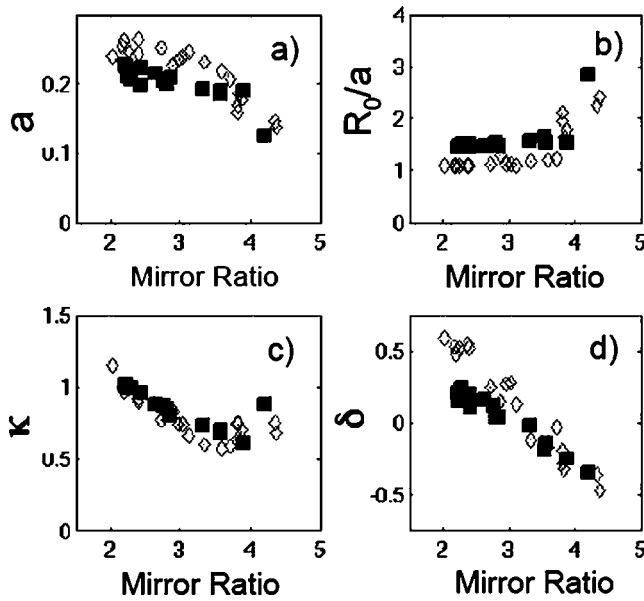
FIG. 13. Plasma shape parameters as derived from the MRXFIT code, The different frames show (a) the minor radius (a), (b) the aspect ratio (R_0/a), (c) the elongation (κ), and (d) the triangularity (δ). These geometric quantities are defined in Eq. (11). Open/closed symbols correspond to discharges without/with the center column.

a large tilt mode, and thus the equilibrium fit should be treated with caution. The equilibrium in Fig. 12(b) is limited on the center column; the mirror ratio (MR=2.5) and elongation (E=0.47) are similar to the previous case. The equilibrium in Fig. 14(c) has an external field mirror ratio of 3.4, yielding a plasma with much smaller elongation (E=0.36). This case displays the strong shaping effect of the shaping coils, which pull the plasma outward. X-points form between the plasma and the shaping coils, and for sufficiently large mirror ratio, these X-points define the plasma boundary. Note the region of good curvature and large field strength outside separatrix and between the shaping coils. It is this region that is postulated to prevent the shift mode from terminating the plasma, as discussed in relation to Fig. 11.

We have computed the equilibria for the set of helium discharges discussed in Sec. IV. The shape parameters for these discharges are illustrated in Fig. 13, where the parameters are defined as:[87]

$$a = (R_o - R_i)/2, \tag{8a}$$

$$R_0 = (R_o + R_i)/2, \tag{8b}$$

$$\kappa = Z_t/a, \tag{8c}$$

$$\delta = (R_0 - R_t)/a, \tag{8d}$$

$$E = (R_o - R_i)/Z_S. \tag{8e}$$

Here, R_i and R_o are the inner and outer radial coordinates, respectively, of the plasma boundary at $Z=0$, and R_t and Z_t are the coordinates of the point with the maximum value of Z on the plasma boundary. Note that the standard FRC definition of elongation (8e) has been modified to account for the fact that these FRC may be limited on the center column.

This FRC definition of elongation (E) is half the value of the definition (κ) commonly used in tokamak research.

The data in Fig. 13 indicate that the plasma shape depends strongly on the mirror ratio of the external field. The minor radius of the plasma tends to be largest when the mirror ratio is smaller, and the aspect ratio is smallest at small mirror ratio. Note that at low mirror ratio, the aspect ratio is consistently smaller without the center column, which limits the plasma when it is present. For large mirror ratio, the plasma is no longer limited by the center column, and the aspect ratio is similar for the two different configurations. The plasma elongation shows a decrease as the mirror ratio is decreased, as does the triangularity. Note that these specific trends are determined by the coil locations in MRX, and do not represent a generic dependence of FRC shape on mirror ratio. Large nonaxisymmetries are typically present for plasma with MR< ~2.8; the equilibrium parameters in these cases should be considered as a good approximation, but not an exact fit. Note that large-mirror-ratio configurations have negative triangularity, which is a novel shape for an FRC. These configurations ($\delta<0$) show the optimum confinement within the database of MRX discharges.

VI. OBLATE FRC STABILITY ANALYSIS

In order to understand the experimental stability results presented in Sec. IV, we have utilized two separate techniques. The first is a rigid-body model for tilting/shifting instabilities,[14] used to provide some intuition regarding $n=1$ modes. The second technique is the use of MHD calculations with the 3D HYM code.[15] These stability analyses will be discussed in this section. Note that both analysis methods rely on equilibria computed with the MRXFIT code.

A. Rigid-body model

We have applied the rigid-body model by Ji *et al.*[14] to the MRX plasmas, in order to assess how the external field shaping impacts the stability to $n=1$ tilt/shift instabilities. This simple model is limited from three perspectives: (1) it assumes rigid-body-like perturbations to the plasma (not the true eigenfunction), (2) it can only approximately account for the stabilizing effect of the center column, and (3) it does not include stabilizing effects such as line tying, compressibility, and viscosity.[60] Nevertheless, the model has the advantage of providing simple physical insight into the nature of FRC global modes.

In this model, the plasma current is broken into a series of rigid current rings which are modeled to tilt or shift in unison with each other. The torque on the plasma is due to the $J \times B$ force between the tilting plasma current rings and the equilibrium field. The torque on the ith current ring due to a small tilt θ_X is given by

$$N_{X,\text{equilibrium},i} = \theta_X \pi R^2 I_i B_{Z,i}(1 - n_{\text{decay},i}), \tag{9}$$

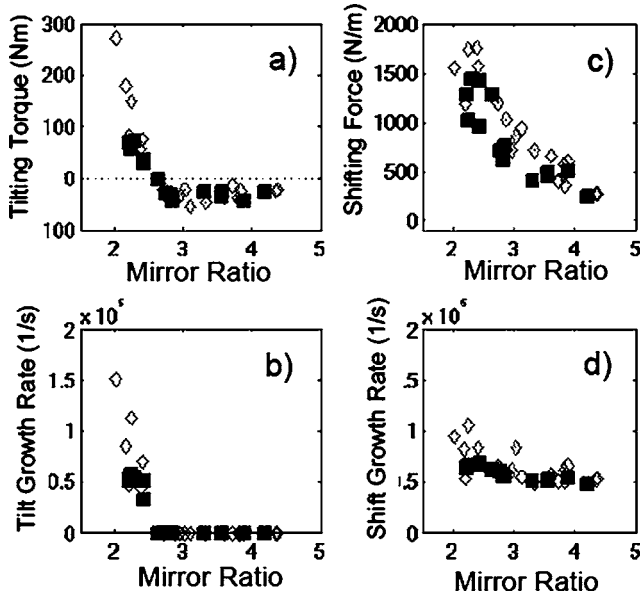where I_i is the current in the ith current ring, and n_{decay} is given by

FIG. 14. Parameters from the rigid-body model for tilting/shifting. The tilting torque and shifting force are illustrated in (a) and (b), while the tilt and shift growth rates are illustrated in (c) and (d). Open/closed symbols are for cases without/with central conductor.
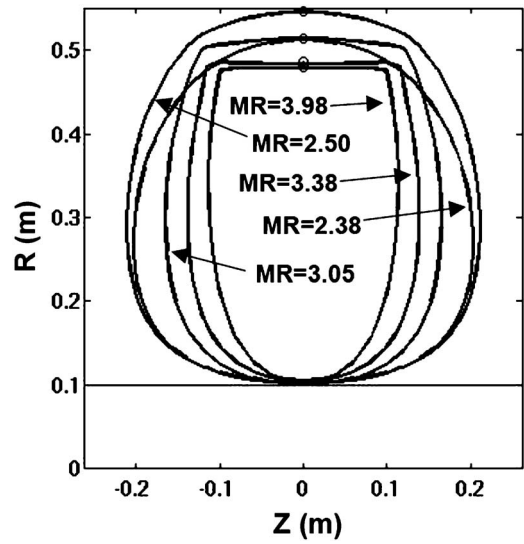

FIG. 15. The five separatrix shapes used in the HYM calculations. The mirror ratio varies from 2.3 to 4 among these shapes. All plasmas are limited by the center column, which is modeled as a perfectly conducting boundary in the simulation.

$$n_{\text{decay}} = -\frac{R}{B_Z}\left[\frac{\partial B_Z}{\partial R} - \frac{Z}{R^2}\frac{\partial}{\partial R}(2RB_R + ZB_Z)\right]. \quad (10)$$

The total torque acting on the plasma is then given by

$$N_{\text{MHD}} = \theta_X \sum_{i=1}^{N_f} \pi R^2 I_i B_{Z,i}(1 - n_{\text{decay},i}). \quad (11)$$

Here, N_f is the number of current filaments making up the plasma current distribution. This torque can act to restore the plasma to its equilibrium position if $n_{\text{decay}} > 1$, or reinforce the tilt-instability if $n_{\text{decay}} < 1$. A small correction to this torque for $n=1$ eddy currents in the center column is applied by modeling an $n=1$ eddy current pattern in the center column using the formulation of Jardin and Christensen.[64]

The growth rate for the tilt instability can then be calculated by solving the equation for the tilt angle:

$$I_X \ddot{\theta}_X = N_X, \quad (12)$$

yielding the solution

$$\theta_X(t) = \theta_{X,0} e^{\gamma t} \quad (13)$$

with

$$\gamma_{\text{tilt}} = \sqrt{\frac{1}{I_X}\sum_{i=1}^{N_f} \pi R^2 |I_i B_{Z,i}|(1 - n_{\text{decay},i})}. \quad (14)$$

Here, I_X is the moment of inertia of the plasma, and is given approximately by treating the plasma as a ring with major and minor radii R_0 and a, respectively, with M_p the total plasma mass:[74]

$$I_X = \frac{M_p}{2}\left[R_0^2 + \frac{5}{4}a^2\right]. \quad (15)$$

A similar derivation leads to the growth rate for radial shifting motion. A plasma that undergoes a small shift ξ will experience a force given by

$$F = -\xi\pi\sum_i \frac{\partial B_Z}{\partial R}R_i I_i. \quad (16)$$

The small shift will be increased or reduced depending on the sign of F. For $F < 0$, the growth rate of the radial shift mode is given by

$$\gamma_{\text{shift}} = \sqrt{\frac{|F|}{M_p}}. \quad (17)$$

The results from these calculation are illustrated in Fig. 16, for the database of helium discharges discussed previously. The tilting torque, normalized to the small displacement θ_X, is illustrated in Fig. 14(a). Note that the torque is positive for mirror ratios <2.5, implying instability to the tilt in this regime. The data in Fig. 6(a) illustrate that MR<2.5 is exactly the regime where large and deadly tilt instabilities occur. For MR>2.5, the measured B_R, $n=1$ amplitudes left over after merging do not grow. Hence, the data and calculation confirm that the very oblate MRX plasmas are indeed in the regime where the tilt mode is stabilized by the equilibrium field alone. The shifting force [Fig. 14(c)], normalized to the displacement ξ, also shows a decrease as the mirror ratio increases. The measured plasma density and calculated plasma volume (hence, the total plasma mass) both decrease with increasing mirror ratio, so that the shifting growth rate, in physical units, is approximately constant with respect to mirror ratio [Fig. 14(d)]. When normalized to the Alfvén time, the shifting growth rate decreases from 1 to 0.3 over the range of mirror ratio displayed in the figure. Note that this model describes the linear stability of the rigid-shift mode and only partially captures the shifting behavior in

MRX: the shifting is observed, but it does *not* grow to the eventual destruction of the configuration.

The rigid-body model[14] also can incorporate the effects of toroidal rotation on the $n=1$ tilt mode. As noted in Sec. IV A, we do not observe strong toroidal rotation in these plasmas, and so have not included this effect in the model. Hence, the dominant stabilizing effect is the strong shaping of the equilibrium field.

There is a third possible rigid-body instability, known as the axial shift,[14] vertical mode, or "roman candle" instability.[1] The strong equilibrium field shaping from the PF windings in the flux-cores generally prevents this instability from being a problem in oblate FRCs in MRX.

B. Stability studies using the HYM code

The equilibria calculated with MRXFIT have been interfaced to the HYM code, providing the initial configuration for stability analyses of these plasmas. The goal of the studies was to (1) determine how the external field and plasma shape impact the linear stability of the FRCs in MRX, and (2) study the possible nonlinear saturation of the radially polarized instabilities.

The linear stability calculation was done for five equilibrium shapes that span the range elongations $0.3 < E < 0.5$ and mirror ratio $2.4 < \mathrm{MR} < 4$, as illustrated in Fig. 15. The MHD linear growth rate for $n = 1–4$ radially and axially polarized modes was computed, starting with an initial axisymmetric equilibrium configuration with an imposed nonaxisymmetric initial perturbation. The simulation region in the axial direction extends between the MRX flux cores ($|z| \leq 40$ cm), and radially up to $R = 72$ cm, thus including the location and effects of the SF coils. Note that the center column is present in all cases, and its effects are included in the HYM calculations.

The computed linear growth rates of axially and radially polarized modes with $1 \leq n \leq 4$ are illustrated in Fig. 16. The growth rate increases as n increases, as expected in the MHD regime.[16,21,28] More importantly, the growth rate of each mode decreases as the elongation is decreased (mirror ratio is increased). Note that tilting (the $n=1$ axially polarized mode) is stable in the accurate linear MHD calculation in all of these cases with a center column. No absolute stability is found in these MHD calculations, due to the everywhere bad curvature of the magnetic field lines.[24]

A separate set of linearized MHD simulations has been performed in order to study the effects of the central conductor on stability and properties of the $n=1$ tilt mode. It was found that the central conductor reduces growth rates of low-n MHD modes ($n \geq 2$), but does not provide complete stabilization for these modes. The $n=1$ tilt mode has been found to be marginally unstable for MRX-FRC with elongation $E = 0.5$ (mirror ratio MR=2.4) without the center column, and it was linearly stable for all more oblate configurations ($E < 0.5$). More accurate comparison of the $n=1$ tilt instability threshold with experimental results (Fig. 6) is complicated by the difficulties of equilibrium reconstruction and poor reproducibility for strongly unstable discharges with small mirror ratio (larger E), as well as approximations made in the
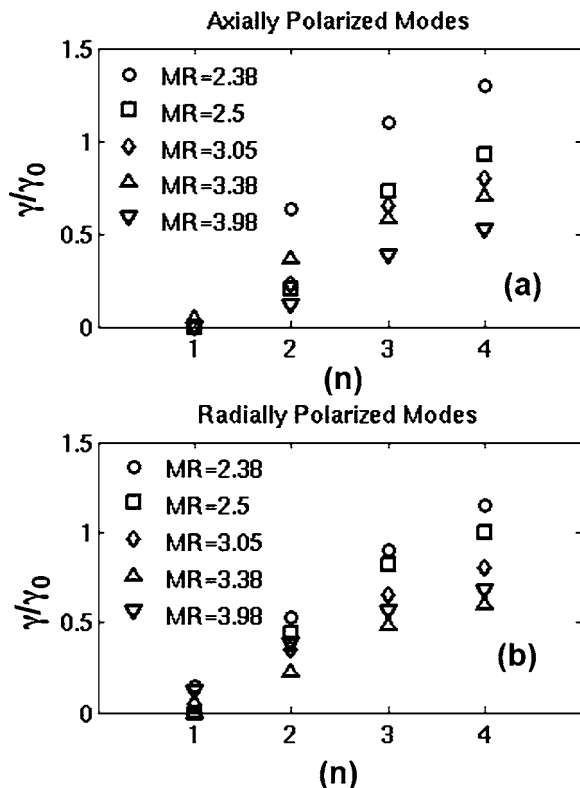

FIG. 16. The growth rate of the axially (a) and radially (b) polarized co-interchange instabilities, as a function of toroidal mode number (n), for the configurations in Fig. 15.
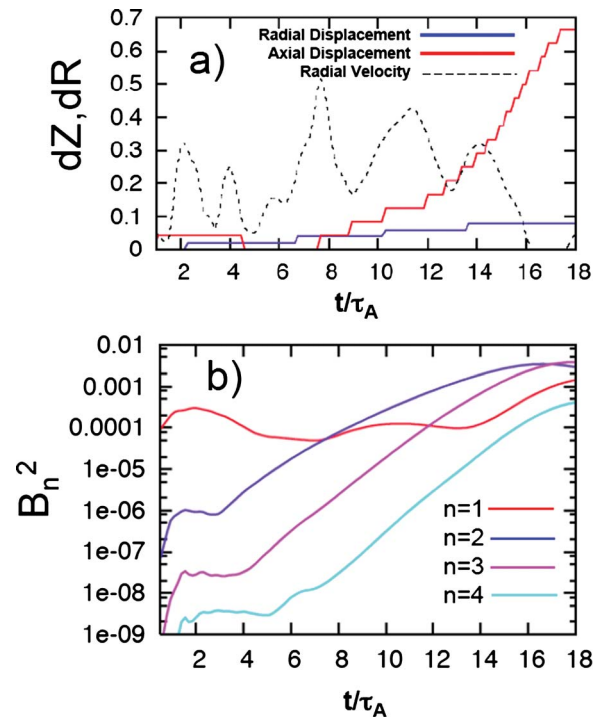

FIG. 17. (Color online) Time evolution plots from nonlinear HYM simulations: (a) Normalized axial shift of the magnetic axis dZ/Z_S (red) and relative radial displacement of plasma boundary at the midplane dR/R_b (blue). The dashed line shows value of radial velocity ($20^*V_R/V_A$) at the plasma boundary. (b) The magnetic energy for $n=1–4$ modes normalized to the total magnetic field energy. Field reversal is lost at $t \sim 13\tau_A$.

HYM simulations (simulations do not include the merging phase of the experiment, and only the region between the flux cores is simulated).

The MRXFIT calculated equilibria have also been used for 3D nonlinear MHD simulations, which have been performed neglecting the center-column effects (Fig. 17). A low mirror-ratio case was simulated, and a large $n=1$ initial perturbation was applied in order to model the strong $n=1$ distortion present in the merging phase of this experiment. In these simulations, the $n=2$ mode was the dominant mode in the initial phase of simulations (compared to other $n>1$ modes), and its amplitude grew comparable to the $n=1$ mode amplitude by $t \sim 7\tau_A$ ($\tau_A = Z_S/V_A$), as shown in Fig. 17(b). The configuration was strongly distorted (not axisymmetric and no field reversal) by $t \sim 13\tau_A$, and after this time the growth of all modes slowed down. At $t \sim 13\tau_A$, all low-n modes ($n=1-3$) had comparable amplitudes $\delta B_R/B_0 \sim 0.1-0.3$ and $\delta B_Z/B_0 \sim 0.2$. Nonlinear simulations for more oblate cases (mirror ratio of 4) show longer lifetimes up to $t \sim 20\tau_A$, even without the center-column stabilization.

In all nonlinear runs, the growth of the radially polarized modes was observed, including the $n=1$ shift mode and other low-n ($n \geq 2$) modes. However, the outward radial displacement associated with these modes was relatively small [Fig. 19(a)]; the plasma remained radially confined inside radius $R < R_{SF}$, where R_{SF} is the shaping coil radius. Figure 17(a) shows time evolution of axial displacement of the magnetic null from the midplane $\Delta Z/Z_s$ (red curve), and the relative shift of the plasma boundary $\Delta R/R_b$ (blue curve), plotted at toroidal angles corresponding to the maximum amplitude axial and radial perturbations, respectively. While the axial shift grows exponentially to values of order of one, the outward radial motion of plasma boundary is limited to small values below 0.1. Figure 17(a) shows time evolution of plasma radial velocity V_R/V_A close to the edge at the midplane (dashed line, scaled by factor of 20). The observed oscillatory behavior of $V_R(t)$ results in a small net radial perturbation of plasma boundary. Analysis of magnetic field perturbation shows that this nonlinear effect is related to compression of the magnetic field lines between the plasma boundary and the SF coils, which prevents further growth of plasma radial displacement. This agrees with experimental observations of plasma radial shift mode (Fig. 11), which "bounces" off the high-field region outside the SF coils. However, the nonlinear simulations without the central conductor do not show complete nonlinear stabilization of radial $n=1-2$ modes. These modes continue to grow inward, resulting in plasma implosion to $r=0$. In the experiments, the center column (not included in the nonlinear HYM simulations) may limit the growth of these modes at small R, resulting in stabilization of the radial co-interchange modes.

We can use these results to estimate the toroidal mode number where FLR effects become important. The condition for finite Larmor radius effect to be important is given by $\gamma \lesssim \omega^*$, where γ is the MHD growth rate and ω^* is the diamagnetic drift frequency given by

$$\omega^* = kv_D = \frac{Tk}{eBL_P}. \tag{18}$$

We utilize the fact that for $\beta=1$, $v_{\text{th},i} = V_a$, and utilize the definition of the gyroradius $\rho_i = m_i v_{\text{th},i}/eB$ to write the diamagnetic drift frequency as

$$\omega^* = kv_D = \frac{n\rho_i V_A}{2R_0 L_P}. \tag{19}$$

The MHD growth rate is $\gamma = CV_A/ER_S$, where C is an order-unity constant to be determined from, for instance, Fig. 16. These expressions can be combined to yield an expression for the n beyond which FLR effect are dominant (utilizing $R_S = 1.44R_0$ and L_P as the distance between the field null and the separatrix):

$$n > \left(\frac{2}{1.44}\right)C\frac{\bar{s}}{E}. \tag{20}$$

For MRX helium parameters, with $C=1$ and $\bar{s}/E \sim 3$, this expression yields $n > 4$. Hence, in MRX, the $n=1$ and 2 instabilities are MHD-like, while modes with $n \geq 3-4$ may begin to display the effects of FLR stabilization.

VII. DISCUSSION AND SUMMARY OF THESE RESULTS

The results presented in this paper present a systematic study of oblate FRC equilibrium and stability, with many comparisons to theoretical and computational expectations. Many of the most significant observations are itemized below.

(1) The $n=2$ and 3 axially polarized co-interchange modes were experimentally identified and shown to be detrimental to FRC performance, even when the tilt was largely stabilized. Although predicted to be MHD unstable, these modes have never previously been identified in an FRC. Kinetic effects in prolate FRCs have probably prevented these modes from being observed; the weaker kinetic effects in the oblate FRC allow these modes to grow more easily. These $n=2$ and 3 axial modes were not strongly affected by the presence of the center conductor, but did respond to the plasma shape. Extremely oblate plasmas had a minimum amplitude of these modes, and the longest lifetime.

(2) As expected,[14,16] the combination of a passive stabilizer and oblate shape leads to the reduction of $n=1$ tilt/shift modes. Note that *both* shaping and the stabilizer were capable of mitigating the deleterious effects of the tilt mode. The elimination of this tilt mode was an important step for extending the lifetime of the FRC, but was not by itself sufficient to prevent rapid destruction of the configuration. A tilt stability boundary at MR=2.5 was predicted based on a rigid-body model, and was found to be in approximate agreement with the measurements in the absence of the center column. Note that neither of these techniques is likely to help eliminate the internal tilt of the prolate FRC.

(3) We have observed the signature of the $n=1$ radial shift mode in the case where there is no center column

present. Interestingly, this mode does not appear to cause a loss of equilibrium and confinement, unlike the $n=1$ tilt. This is most likely because the plasma torus is reflected from the strong field in the region outside shaping coils.

(4) Further verification is shown that spheromak merging is a viable method for forming FRC plasmas. This technique has been now been verified for spheromaks formed by plasma guns (TS-3[88] and SSX[37]), Z-θ discharges (TS-3[34]), and flux-cores (TS-4[36] and MRX). The merging process has been stabilized with a conducting center column (TS-3/4 and MRX), a flux-conserver (SSX), and merging has been demonstrated with no stabilization at all (MRX,[89] and this paper). There now exists a large variety of FRC formation techniques. For the prolate case, the theta-pinch,[1] RMF,[90] and co-axial slow-source (CSS) technique,[91] have demonstrated FRC formation. Oblate FRCs have been formed by spheromak merging and the bias field/laser plasma/fast coil combination of Nakata *et al.*,[55,56] and it is likely that translation of a theta-pinch formed FRC into an oblate confinement chamber would work as well.[92]

(5) The MHD equilibrium was studied for plasmas with different external field shapes. It was found that as the mirror ratio was increased (leading to longer lifetime), the minor radius, elongation, and triangularity of the plasma all decreased. These results demonstrate the ability to modify the oblate FRC shape in a controlled manner through the use of equilibrium field shaping.

(6) The linear stability for $n \geq 2$ co-interchange modes was studies using both the HYM code and a simple model for the local mode growth rate. These calculations predicted that the configurations at large mirror ratio should be more stable to local modes, in agreement with measurements. Nonlinear simulations using HYM code have shown that outward growth of radial displacement (due to radially polarized instabilities with $n \geq 1$) is limited in the nonlinear regime due to compression of magnetic field between the plasma boundary and SF coils, consistent with experimental findings.

There are many outstanding issues that must be addressed in order to further understand the fusion relevance of these oblate FRC configurations. These include, but are not limited to, plasma sustainment techniques and stability studies for longer plasma lifetimes.

The most critical issue for the present line of research is probably the sustainment of the configuration for much longer than the current diffusion and particle and energy confinement times. Both an ohmic solenoid and neutral beam injection (NBI)[93] are possible means of sustaining the oblate FRC plasma. Successful sustainment of both FRC[94] and spheromak[95] plasmas with an ohmic solenoid has been demonstrated in previous experiments. Successful neutral beam injection into an FRC has been demonstrated in the FIX device, where an improvement in plasma confinement was observed with NBI.[96,97] These two sustainment methods, NBI and ohmic drive, are utilized in the proposed SPIRIT concept.[98,99] Note that repetitive spheromak merging has also been suggested as a means of oblate FRC sustainment,[35] as
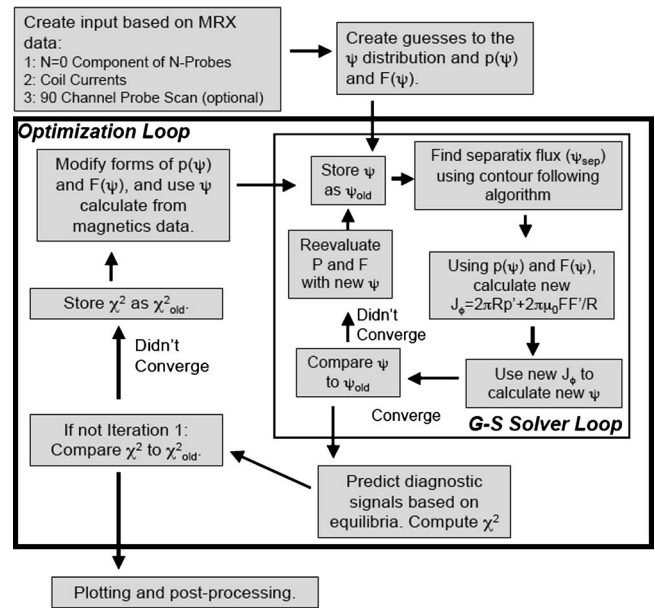

FIG. 18. Algorithm of the MRXFIT code.

has the thermoelectric effect.[100] In prolate FRC research, the topic of a rotating magnetic field (RMF) current drive has been studied, with promising results[90] for FRC startup and sustainment.

Also of critical importance is the elimination of MHD instability for the duration of the sustained period. The neutral beam in the SPIRIT concept serves this important role in the oblate case: stabilization of $n \geq 2$ co-interchange modes.[20] Experiments reported in this paper have demonstrated the reduction of $n=2$ and 3 axially polarized modes through highly oblate shaping of the plasma. It would be desirable to have a more spherical plasma shape ($E \sim 0.6-1$), a configuration that is predicted (Ref. [16]) and measured (this paper) to be unstable to $n \geq 2$ axially polarized co-interchange modes. Recent numerical simulations have indicated that the presence of a nonthermal beam distribution can stabilize the $n \geq 2$ co-interchange modes. Indeed, FRC configurations stable to all macroscopic modes have been found when a sustained plasma (ohmically or otherwise) is stabilized with a high-energy particle beam.[16] The present research provides a first step toward these promising configurations. For the prolate case, note that the active stabilization of the $n=2$ rotational mode was achieved using RMF[54] or multipole fields.[52,53]

In summary, we have studied the stability properties of oblate FRCs formed by spheromak merging. These studies were performed with different external field shapes, and both with and without a stabilizing center conductor. The results show the plasma to be unstable to $n=1$ tilt/shift modes when the center conductor is absent. The presence of the center conductor and/or oblate shaping leads to the elimination of the $n=1$ tilt, while the $n=1$ shift is stabilized by the center conductor. These steps are not sufficient to form a long-lived FRC, because $n \geq 2$ modes quickly grow, terminating the plasma. These co-interchange modes can be largely suppressed by forming very oblate plasmas, which are measured
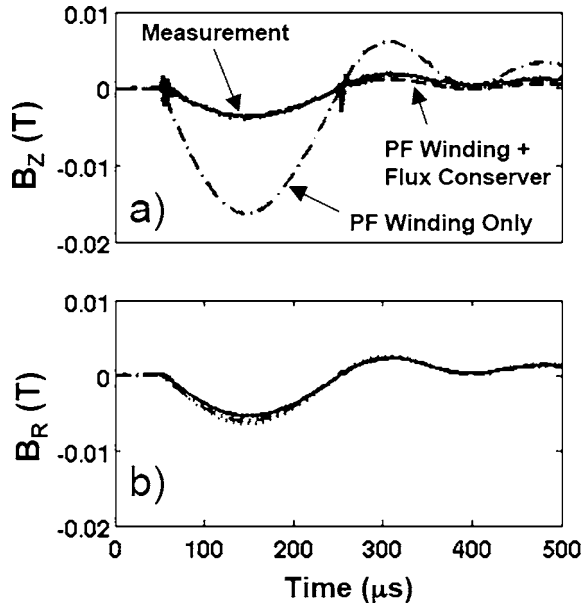
FIG. 19. Measured and predicted magnetic fields: (a) B_Z and (b) B_R for one of the coil triplets of the 90-channel probe. The measured magnetic field is shown in the black line, the prediction with only the PF windings is draws with a dot-dashed line (---), and the prediction with the PF windings and flux conserver is shown with a dashed line (---), The prediction using the flux conserving vessel accurately matches the measurement.

to have the minimal $n=2$ and 3 activity and the longest lifetime. The equilibria of these plasmas have been calculated by finding a solution to the Grad-Shafranov equation constrained by the available magnetics data. The equilibrium calculations clearly indicate that the plasma becomes more oblate as the external field mirror ratio is increased, and demonstrate control of the FRC boundary. A rigid-body model has shown that these very oblate plasmas are in the MHD tilt-stable regime. Calculations of the MHD linear growth rate with the HYM code that the oblate plasmas have improved stability with respect to both radially and axially polarized co-interchange instabilities. These results indicate how detailed control of the plasma shape, in addition to passive stabilization, can improve the stability of the oblate FRC plasma.

APPENDIX A: DETAILS OF THE EQUILIBRIUM FITTING PROCEDURE

This appendix presents some details of the equilibrium fitting techniques utilized in the MRXFIT code.

The structure of the MRXFIT code is illustrated in Fig. 18. The fitting process begins with fitting the available magnetic data to the analytic Grad-Shafranov (G-S) solution by Zheng.[89] This solution provides a good initial guess to the poloidal flux distribution and the profiles $p(\psi)$ and
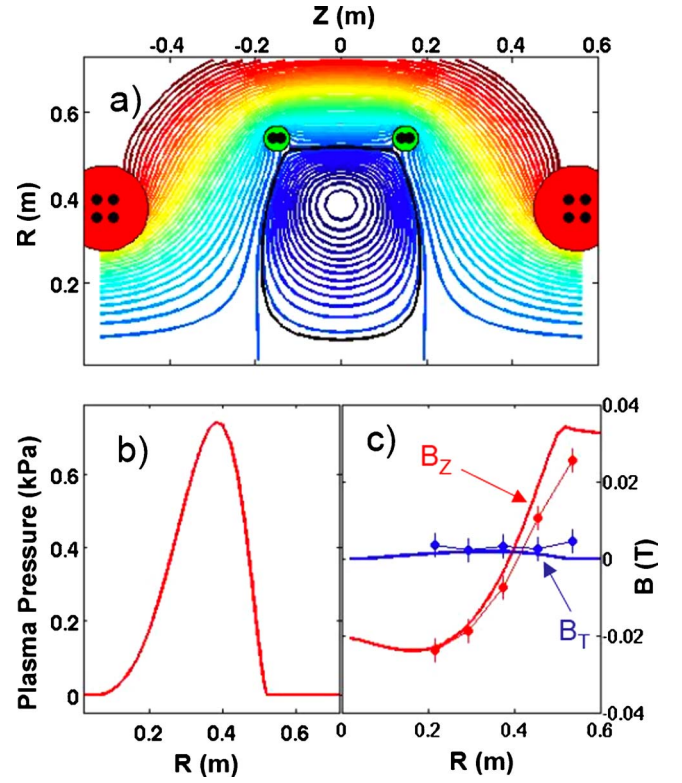

FIG. 20. (Color online) Reconstruction of an FRC in MRX, for a case with a mirror ratio of 2.9. The reconstructed poloidal flux contours are illustrated in (a) and the pressure profile is plotted in (b). The measured and fit midplane magnetic profiles are illustrated in (c).

$F(\psi)F'(\psi)$. These profiles are mapped to the model profiles

$$p'(\psi) = \sum_{i=1}^{N_p} A_i \hat{\psi}^{\alpha_i}, \tag{A1a}$$

$$FF'(\psi) = C\hat{\psi}^\gamma, \tag{A1b}$$

where A_i, C, α_i, and γ are free parameters to be adjusted, N_p is the number of terms in the pressure profile (typically $N_p = 1$ or 2), and $\hat{\psi}$ is defined as

$$\hat{\psi} = \frac{\psi - \psi_{\text{sep}}}{\psi_{\text{axis}} - \psi_{\text{sep}}}. \tag{A2}$$

The G-S equation is then solved for these parameters, using an iterative technique described in Ref. 75 and illustrated in Fig. 18. The solution to the G-S equation provides a distribution of plasma current, which, in combination with the coil currents, is used to calculation the magnetic field. This magnetic field is compared to the measured field, and the value of χ^2 is calculated as

$$\chi^2 = \sum_k \frac{(B_{k,\text{pred}} - B_{k,\text{meas}})^2}{\sigma_k^2}. \tag{A3}$$

Here, $B_{k,\text{pred}}$ is the prediction for the kth magnetic signal based on the G-S solution, $B_{k,\text{meas}}$ is the measured kth signal, and σ_k is the uncertainty in the kth measurement. The fit parameters are then repeatedly varied, with the goal of minimizing the value of χ^2. This minimization process is con-
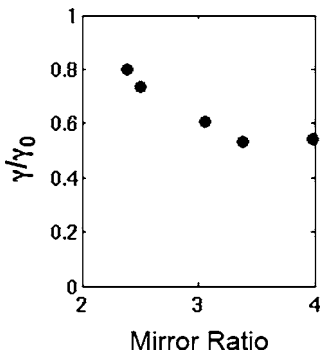
FIG. 21. The growth rate of "local modes," as a function of mirror ratio, based on Eq. (B4). The growth rate is reduced as the plasma shape becomes more oblate.

trolled with the MATLAB fminsearch function, which uses a Nelder-Mead simplex method.

One complication in the free-boundary algorithm is the determination of the separatrix at each iteration of the G-S solution algorithm. In the present code, contours of constant poloidal flux are found with the MATLAB contourc function. The separatrix is determined as the contour with maximum flux which surrounds the magnetic axis, does not link the shaping-field coils, and does not cross the center column if it is present (note that the poloidal flux at the field null is negative in the MRX convention). Hence, it is possible for the equilibria to be center-column limited, shaping coil limited, or to have a separatrix not limited by any physical structure. The latter happens for low mirror ratio without the center column, or for large mirror ratio where a pair of X-points form near the shaping coils. No plasma pressure or currents are allowed outside the plasma boundary.

The fast time scale of the discharge presents a challenge for the calculation of the magnetic field in the equilibrium modeling. As noted in Sec. III, the equilibrium field is provided by a superposition of the steady state EF coils outside the vacuum vessel and the fast shaping-field coils and poloidal field windings of the flux cores. The steady state field of the EF coils is able to penetrate the vacuum vessel long before the plasma starts. On the other hand, the flux from the internal coils is not able to penetrate the vacuum vessel, which thus acts as a perfect flux conserver. We utilize the external poloidal flux loops to monitor the flux leaking through the vacuum vessel, and measure that at most 2% of the poloidal flux from the PF windings leaks through the vacuum vessel on the discharge time scale.

In order to account for the flux-conserving nature of the vacuum vessel, we have utilized flux-conserving Green's tables. These Green's tables precompute the field on the computational grid, with the vacuum vessel treated as a perfect flux-conserver, as detailed in Ref. 75. Separate tables are constructed for the currents in the PF windings, SF coils, EF coils, and plasma currents on the computational grid itself. In addition, diagnostic Green's tables have been computed which quickly map the different coil and plasma currents to the fields at the magnetic diagnostics.

An example of these diagnostic Green's table usage is illustrated in Fig. 19. Only the PF windings are fired in this

discharge; no plasma is present. The measured B_Z and B_R fields at one location of the 90-channel probe are illustrated, as well as two calculations for each measurement. The field calculated without including the effects of the vacuum vessel ("PF Winding Only") clearly overestimates the actual magnetic field, while the field calculated with the flux-conserving vessel is much more accurate in predicting the measurement. The B_Z field is more strongly impacted by the vacuum vessel currents than B_R, because the vacuum vessel acts in essence as a large solenoid canceling part of the B_Z from the fast internal coils. Note that these flux-conserving calculations are utilized in computing the external field shape and mirror ratio for all cases described in this paper.

There are two distinct magnetic probe arrays which can provide magnetic constraints on these equilibrium calculations: the 90-channel probe array and the toroidally distributed probe array (N-probes). The data from the 90-channel probe array suffer from its nonaxisymmetric nature: it only contains information about a single toroidal angle. The data from Sec. IV indicate that even in the best cases, substantial nonaxisymmetries exist in MRX, making it questionable to constrain the fits by data from a single toroidal angle. On the other hand, the $n=0$ components of B_Z and B_T from the toroidally distributed probe array are by definition axisymmetric, and provide strong constraints on the equilibrium. Hence, only the information from the toroidally distributed array is typically used to constrain the equilibrium. The $n=0$ component of B_R is zero for these up-down symmetric equilibria. The poloidal flux loops on the vacuum vessel are not useful as a constraint because a flux-conserving vessel model is used.

The final result of the these calculations are the poloidal flux in the R-Z plane and the profiles $p(\psi)$ and $FF'(\psi)$. All other useful quantities can be derived from this information. An example reconstruction is shown in Figs. 20(a)–(c). The equilibria in Fig. 20(a) are for a discharge without a center conductor; a pair of X-points forming near the shaping coils determines the separatrix in this case. This discharge has a maximum pressure of ~650 Pa (assuming that the pressure at the plasma boundary is zero). This is approximately consistent with the single point kinetic pressure of 600 Pa. This equilibrium has a plasma boundary elongation of 0.41 and an aspect ratio of 1.3. The total current is 27 kA, leading to a trapped flux of 7.1 mWb. The midplane profiles of B_Z and B_T are illustrated in Fig. 20(c). The is a small residual B_t present, but $q < 0.05$ at all radii, where the safety factor is defined as $q = d\Phi/d\psi$ with Φ the toroidal flux.[49]

APPENDIX B: LOCAL MODE STABILITY ANALYSIS

We estimate the stability to high-n co-interchange modes ($n \to \infty$), based on the local mode formulation in Ishida *et al.*[29] They noted that the approximate growth rate of local modes could be calculated from the variational principle

$$\omega^2 = \frac{\partial W}{T}. \tag{B1}$$

For a pure displacement [Eq. (3) of Ref. 24], the kinetic energy is bounded by the quantity

$$\partial W = -\frac{1}{2}\frac{\partial}{\partial \psi}\oint dl\kappa RB^2, \tag{B2}$$

where $\kappa = -\hat{\psi}\cdot(\hat{b}\cdot\nabla)\hat{b}$ is the normal curvature vector.[24] The inertia term (T) is calculated by inserting the pure displacement into the form for the inertial term [Eq. (6) of Ref. 28], and taking the large toroidal mode number limit. The resulting inertial term is given by

$$T = 2\pi \oint \frac{dl}{B}. \tag{B3}$$

Inserting (B2) and (B3) into (B1) yields an expression for the local mode growth rate ω:

$$\omega^2 = \frac{-\dfrac{1}{2}\dfrac{\partial}{\partial \psi}\oint dl\kappa RB^2}{2\pi \oint \dfrac{dl}{B}}. \tag{B4}$$

This formulation has been shown to provide a reasonably approximate means of estimating the growth rate of the most unstable local mode in prolate FRCs.[29] Note that these local modes are not necessarily expected to lead to the violent termination of the plasma; they may result instead in enhanced transport and a resulting fast decay of the configuration.

The data in Fig. 21 illustrate the local mode growth rate from Eq. (B4). There is a clear reduction in the growth rate as the mirror ratio is increased (more oblate shape), although the effect appears to saturate at large mirror ratio. The growth rates from the HYM calculations (Fig. 18) are similar to these predictions, though two caveats should be remembered in making this comparison: (i) the "pure displacement" is not the true eigenfunction of the most unstable mode, unlike HYM, which calculates the growth rate of the most unstable mode, and (ii) the HYM calculations in Fig. 18 are for modes with $n \leq 4$, whose MHD growth rates will be less than the $n \rightarrow \infty$ limit. Nevertheless, within its domain of applicability, the simple model predicts the reduction in the co-interchange growth rate for more oblate plasmas.

[1] M. Tuszewski, Nucl. Fusion **28**, 2033 (1988).
[2] H. Momota, A. Ishida, Y. Kohzaki, G. H. Miley, S. Ohi, M. Ohnishi, K. Yoshikawa, K. Sato, I. C. Steinhauer, Y. Tomita, and M. Tuszewski, Fusion Technol. **21**, 2307 (1992).
[3] H Y. Guo, A. L. Hoffman, K. E. Miller, and L. C. Steinhauer, Phys. Rev. Lett. **92**, 245001 (2004).
[4] H. Himura, A. Okada, S. Sugimoto, and S. Goto, Phys. Plasmas **2**, 191 (1995).
[5] T. Intrator, S. Y. Zhang, J. H. Degnan, I. Furno, C. Grabowski, S. C. Hsu, E. L. Ruden, P. G. Sanchez, J. M. Taccetti, M. Tuszewski, W. J. Waganaar, and G. A. Wurden, Phys. Plasmas **11**, 2580 (2004).
[6] M. N. Rosenbluth and M. N. Bussac, Nucl. Fusion **19**, 489 (1979).
[7] J. H. Hammer, Nucl. Fusion **21**, 488 (1981).
[8] J. L Schwarzmeier, D. C. Barnes, D. W. Hewett, C. E. Seyler, A. I. Shestakov, and R. L. Spencer, Phys. Fluids **26**, 1695 (1983).
[9] R. A. Clemente and J. L. Milovich, Phys. Fluids **26**, 1874 (1983).
[10] D. C. Barnes, J. L. Schwarzmeier, H. R. Lewis, and C. L. Seyler, Phys. Fluids **29**, 2616 (1986).
[11] A. Ishida, H. Momota, and L. C. Steinhauer, Phys. Fluids **31**, 3024 (1988).
[12] R. D. Milroy, D. C. Barnes, R. C. Bishop, and R. B. Webster, Phys. Fluids B **1**, 1225 (1989).
[13] R. Horiuchi and T. Sato, Phys. Fluids B **1**, 581 (1989).
[14] H. Ji, M. Yamada, R. Kulsrud, N. Pomphrey, and H. Himura, Phys. Plasmas **5**, 3685 (1998).
[15] E. Belova, S. C. Jardin, H. Ji, M. Yamada, and R. Kulsrud, Phys. Plasmas **7**, 4996 (2000).
[16] E. Belova, S. C. Jardin, H. Ji, M. Yamada, and R. Kulsrud, Phys. Plasmas **8**, 1267 (2001).
[17] N. Iwasawa, A. Ishida, and L. C. Steinhauer, Phys. Plasmas **8**, 1240 (2001).
[18] E. Belova, R. C. Davidson, H. Ji, and M. Yamada, Phys. Plasmas **10**, 2361 (2003).
[19] E. Belova, R. C. Davidson, H. Ji, and M. Yamada, Phys. Plasmas **11**, 2523 (2004).
[20] E. Belova, R. C. Davidson, H. Ji, and M. Yamada, Phys. Plasmas **13**, 056115 (2006).
[21] I. B. Bernstein, E. A. Freiman, M. D. Kruskal, and R. M. Kulsrud, Proc. R. Soc. London, Ser. A **244**, 17 (1958).
[22] L. Sparks, J. M. Finn, and R. N. Sudan, Phys. Fluids **23**, 611 (1980).
[23] W. A. Newcomb, Phys. Fluids **23**, 2296 (1980).
[24] J. R. Cary, Phys. Fluids **24**, 2239 (1981).
[25] P. L. Pritchett, Phys. Fluids **24**, 864 (1981).
[26] J. Finn, Phys. Fluids **24**, 274 (1981).
[27] D. V. Anderson and D. C. Barnes, J. Comput. Phys. **42**, 288 (1981).
[28] A. Ishida, N. Shibata, and L. C. Steinhauer, Phys. Plasmas **1**, 4022 (1994).
[29] A. Ishida, N. Shibata, and L. C. Steinhauer, Phys. Plasmas **3**, 4278 (1996).
[30] M. Tuszewski, D. C. Barnes, R. E. Chrien, J. W. Cobb, D. J. Rej, R. E. Siemon, D. P. Taggart, and B. L. Wright, Phys. Rev. Lett. **66**, 711 (1991).
[31] M. Tuszewski, D. P. Taggart, R. E. Chrien, D. J. Rej, R. E. Siemon, and B. L. Wright, Phys. Fluids B **3**, 2856 (1991).
[32] J. T. Slough, A. L. Hoffman, R. D. Milroy, E. A. Crawford, M. Cecik, R. Maqueda, G. A. Wurden, Y. Itoh, and A. Shiokawa, Phys. Rev. Lett. **69**, 2212 (1992).
[33] J. T. Slough and A L. Hoffman, Phys. Fluids B **5**, 4366 (1993).
[34] Y. Ono, M. Inomoto, Y. Ueda, T. Matsuyama, and T. Okazaki, Nucl. Fusion **39**, 2001 (1999).
[35] Y. Ono, T. Matsuyama, K. Umeda, and E. Kawamori, Nucl. Fusion **43**, 649 (2003).
[36] E. Kawamori and Y. Ono, Phys. Rev. Lett. **95**, 085003 (2005).
[37] C. D. Cothran, A. Falk, A. Fefferman, M. Landreman, M. R. Brown, and M. J. Schaffer, Phys. Plasmas **10**, 1748 (2003).
[38] K. F. McKenna, W. T. Armstrong, R. R. Bartsch, R. E. Chrien, J. C. Cochrane, Jr., R. W. Kewish, Jr., P. Klinger, R. K. Linford, D. J. Rej, E. G. Sherwood, R. E. Siemon, and M. Tuszewski, Phys. Rev. Lett. **50**, 1787 (1983).
[39] M. Yamada, H. Ji, S. Hsu, T. Carter, R. Kulsrud, N. Bretz, F. Jobes, Y. Ono, and F. Perkins, Phys. Plasmas **4**, 1936 (1997).
[40] R. N. Sudan and E. Ott, Phys. Rev. Lett. **33**, 355 (1974).
[41] R. V. Lovelace, Phys. Fluids **19**, 723 (1976).
[42] A. Friedman, R. N. Sudan, and J. Denavit, Phys. Fluids **29**, 3317 (1986).
[43] L. Sparks and R. N. Sudan, Phys. Fluids **27**, 626 (1984).
[44] C. B. Ruchti and R. V. Lovelace, Phys. Fluids **27**, 1789 (1984).
[45] W. T. Armstrong, R. K. Linford, J. Lipson, D. A. Platts, and E. G. Sherwood, Phys. Fluids **24**, 2068 (1981).
[46] M. N. Rosenbluth, N. A. Krall, and N. Rostoker, Nucl. Fusion Suppl. **1**, 143 (1962).
[47] G. Bateman, *MHD Instabilities* (MIT Press, Cambridge, Massachusetts, 1978).
[48] J. Freidberg, *Ideal Magnetohydrodynamics* (Plenum, New York, 1987).
[49] J. Wesson, *Tokamaks* (Clarendon, Oxford, 1987).
[50] A. M. M. Todd, M. S. Chance, J. M. Greene, R. C. Grimm, J. L. Johnson, and J. Manickam, Phys. Rev. Lett. **38**, 826 (1977).
[51] M. Tuszewski, Plasma Phys. Controlled Fusion **26**, 991 (1984).
[52] S. Ohi, T. Minato, Y. Kawakami, M. Tanjyo, S. Okada, T. Ito, M. Kako, S. Goto, T. Ishimura, and H. Ito, Phys. Rev. Lett. **51**, 1042 (1983).
[53] A. L. Hoffman, J. T. Slough, and D. G. Harding, Phys. Fluids **26**, 1626 (1983).
[54] H. Y. Guo, A. L. Hoffman, R. D. Milroy, K. E. Miller, and G. R. Votroubek, Phys. Rev. Lett. **94**, 185001 (2005).
[55] S. Nakata, T. Sekiguchi, and M. Isaka, Phys. Fluids **28**, 445 (1985).
[56] S. Nakata, T. Sekiguchi, H. Seki, and K. Yamamoto Phys. Fluids **29**, 871 (1986).
[57] M. Yamada, Y. Ono, A. Hayakawa, M. Katsurai, and F. W. Perkins, Phys. Rev. Lett. **65**, 721 (1990).
[58] Y. A. Omelchenko, M. J. Schaffer, and P. B. Parks, Phys. Plasmas **8**, 4463

(2001).

[59] Y. A. Omelchenko, Phys. Plasmas **7**, 1443 (2000).

[60] E. V. Belova, R. C. Davidson, H. Ji, M. Yamada, C. D. Cothran, M. R. Brown, and M. J. Schaffer, Nucl. Fusion **46**, 162 (2006).

[61] T. R. Jarboe, I. Henins, H. W. Hoida, R. K. Linford, J. Marshal, D. A. Platts, and A. R. Sherwood, Phys. Rev. Lett. **45**, 1264 (1980).

[62] T. R. Jarboe, Phys. Plasmas **12**, 058103 (2005).

[63] C. P. Munson, A. Janos, F. Wysocki, and M. Yamada, Phys. Fluids **28**, 1525 (1985).

[64] S. C. Jardin and U. Christensen, Nucl. Fusion **21**, 1665 (1981).

[65] M. Yamada, H. Ji, S. Hsu, T. Carter, R. Kulsrud, Y. Ono, and F. Perkins, Phys. Rev. Lett. **78**, 3117 (1997).

[66] H. Ji, M. Yamada, S. Hsu, and R. Kulsrud, Phys. Rev. Lett. **80**, 3256 (1998).

[67] S. C. Hsu, G. Fiksel, T. A. Carter, H. Ji, R. Kulsrud, and M. Yamada, Phys. Rev. Lett. **84**, 3859 (2000).

[68] T. C. Carter, H. Ji, F. Trintchouk, M. Yamada, and R. Kulsrud, Phys. Rev. Lett. **88**, 015001 (2002).

[69] H. Ji, S. Terry, M. Yamada, R. Kulsrud, A. Kuritsyn, and Y. Ren, Phys. Rev. Lett. **92**, 115001 (2004).

[70] Y. Ren, M. Yamada, S. P. Gerhardt, H. Ji, R. Kulsrud, and A. Kuritsyn, Phys. Rev. Lett. **95**, 055003 (2005).

[71] M. Yamada, H. P. Furth, W. Hsu, A. Janos, S. Jardin, M. Okabayashi, J. Sinnis, T. H. Stix, and K. Yamazaki, Phys. Rev. Lett. **46**, 188 (1981).

[72] I. H. Hutchinson, *Principles of Plasma Diagnostics* (Cambridge University Press, New York, 2002).

[73] A. Thorne, U. Litzen, and S. Johansson, *Spectrophysics* (Springer, Berlin, 1999).

[74] C. P. Munson, "Experimental Identification and Control of Spheromak Tilting Instabilities," Ph.D. thesis, Princeton University, 1983.

[75] Both the name and structure of this code closely follow the MSTFIT code, described in J. K. Anderson, C. B. Forest, T. M. Biewer, J. S. Sarff, and J. C. Wright, Nucl. Fusion **44**, 162 (2004).

[76] L. L. Lao, H. St. John, R. D. Stambaugh, A. G. Kellman, and W. Pfeiffer, Nucl. Fusion **25**, 1611 (1985).

[77] L. L. Lao, J. R. Ferron, R. J. Groebner, W. Howl, H. St. John, E. J. Strait, and T. S. Taylor, Nucl. Fusion **30**, 1035 (1990).

[78] L. C. Appel, M. K. Bevir, and M. J. Walsh, Nucl. Fusion **41**, 169 (2001).

[79] S. Sabaugh, S. M. Kaye, J. Menard, F. Paoletti, M. Bell, R. E. Bell, J. M. Bialek, M. Bitter, E. D. Fredcickson, D. A. Gates, A. H. Glasser, H. Kugel, L. L. Lao, B. P. LeBlanc, R. Maingi, R. J. Maqueda, E. Mazzucato, D. Mueller, M. Ono, S. F. Paul, M. Peng, C. H. Skinner, D. Stutman, G. A. Wurden, W. Zhu, and NSTX Research Team, Nucl. Fusion **41**, 1601 (2001).

[80] D. M. Willett, P. K. Browning, S. Woodruff, and K. J. Gibson, Plasma Phys. Controlled Fusion **41**, 595 (1999).

[81] M. V. Umansky, R. H. Bulmer, D. N. Hill, L. L. LoDestro, H. S. McLean, W. M. Nevins, D. D. Ryutov, and S. Woodruff, Plasma Phys. Controlled Fusion **48**, 235 (2006).

[82] R. L. Spencer and D. W. Hewett, Phys. Fluids **25**, 1365 (1982).

[83] D. W. Hewett and R. L. Spencer, Phys. Fluids **26**, 1299 (1983).

[84] R. l. Spencer and M. Tuszewski, Phys. Fluids **28**, 1810 (1985).

[85] Y. Suzuki, S. Okada, and S. Goto, Phys. Plasmas **7**, 4062 (2000).

[86] T. Takahashi, H. Gota, and Y. Nogi, Phys. Plasmas **11**, 4462 (2004).

[87] S. B. Zheng, A. J. Wooten, and E. R. Solano, Phys. Plasmas **3**, 1176 (1996).

[88] Y. Ono, A. Morita, and M. Katsurai, Phys. Fluids B **5**, 3691 (1993).

[89] M. Yamada, H. Ji, T. A. Carter, S. C. Hsu, R. M. Kulsrud, N. L. Bretz, F. C. Jobes, Y. Ono, M. Katsurai, T.-H. Watanabe, T. Sato, and T. Hayashi, *16th IAEA Fusion Energy Conference*, Montreal, Canada (International Atomic Energy Agency, Vienna, 1996), Paper IAEA-CN-64/CP-19.

[90] A. L. Hoffman, H. Y. Guo, K. E. Miller, and R. D. Milroy, Phys. Plasmas **13**, 012507 (2006).

[91] Z. A. Pietrzyk, G. C. Vlases, R. D. Brooks, K. D. Hahn, and R. Raman Nucl. Fusion **27**, 1478 (1987).

[92] J. Slough (private communication).

[93] A. F. Lifschitz, R. Farengo, and A. L. Hoffman, Nucl. Fusion **44**, 1015 2004.

[94] Y. Ono, A. Morita, T. Itagaki, and M. Katsurai, *Plasma Physics and Controlled Nuclear Fusion Research 1992, 14th IAEA Fusion Energy Conference*, Würzburg, Germany (International Atomic Energy Agency, Vienna, 1993), Vol. 2, p. 619.

[95] P. E. Young, F. J. Wysocki, M. Yamada, and A. Janos, Phys. Fluids B **3**, 2591 (1991).

[96] T. Asai, Y. Suzuki, T. Yoneda, F. Kodera, M. Okubo, S. Okada, and S. Goto, Phys. Plasmas **7**, 2294 (2000).

[97] S. Okada, T. Asai, F. Kodera, K. Kitano, Y. Suzuki, K. Yamanaka, T. Kanki, M. Inomoto, S. Yoshimura, M. Okubo, S. Sugimoto, and S. Goto, Nucl. Fusion **41**, 625 (2001).

[98] H. Ji and M. Yamada, J. Plasma Fusion Res. **2**, 196 (1999).

[99] M. Yamada, H. Ji, E. V. Belova, S. P. Gerhardt, R. C. Davidson, and D. R. Mikkelsen, J. Plasma Fusion Res. (submitted).

[100] A. B. Hassam, R. M. Julsrud, R. J. Goldston, H. Ji, and M. Yamada, Phys. Rev. Lett. **83**, 2969 (1999).